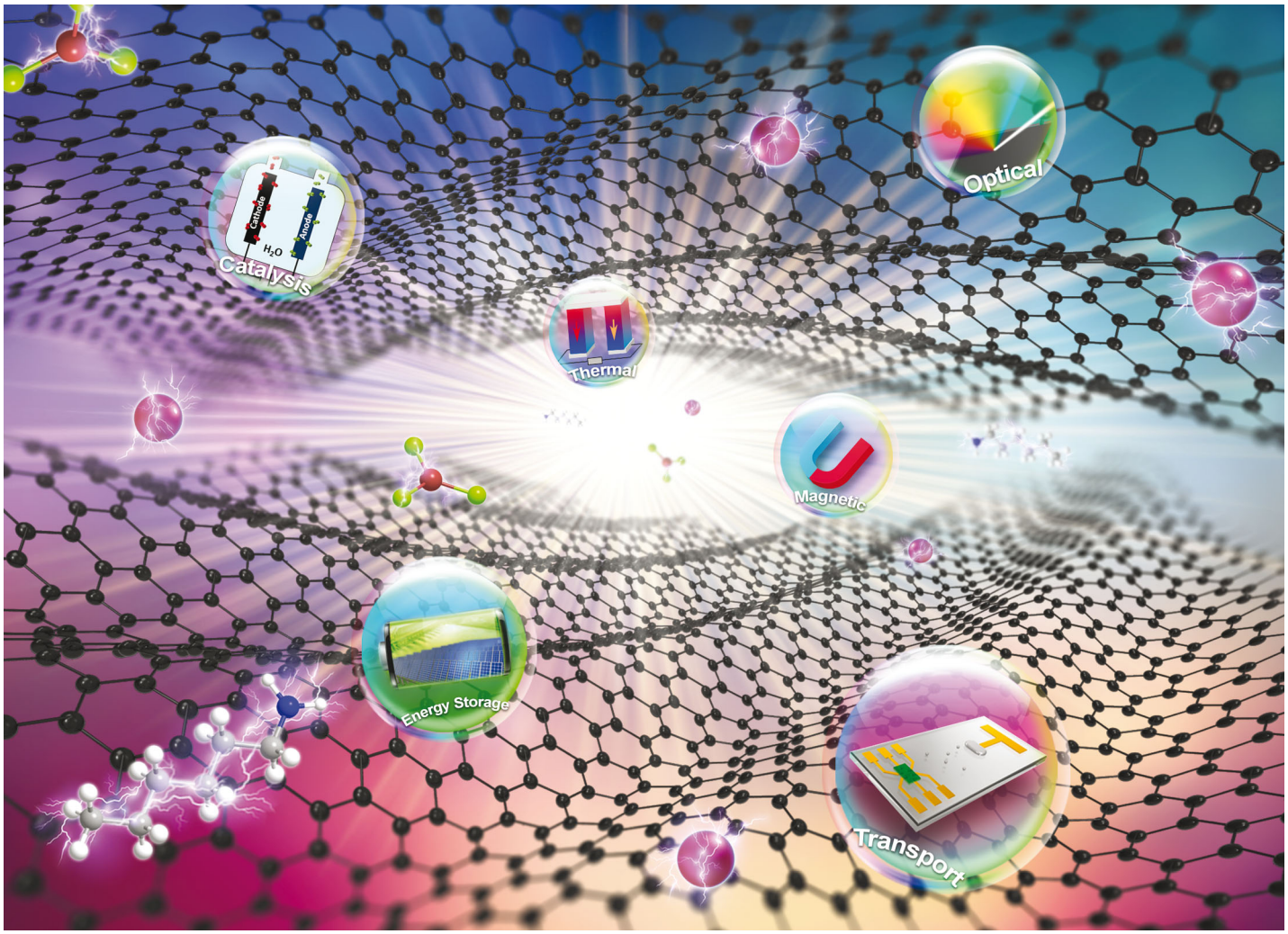

Featuring work from the research group of Professor Liangbing Hu, University of Maryland, USA.

Tuning two-dimensional nanomaterials by intercalation: materials, properties and applications

Intercalations of various species (organic and inorganic) in 2D layered materials lead to drastic tuning of a variety of their physical and chemical properties.

As featured in:

See Liangbing Hu *et al.*, *Chem. Soc. Rev.*, 2016, **45**, 6742.

ROYAL SOCIETY OF CHEMISTRY

www.rsc.org/chemsocrev

Registered charity number: 207890

Chem Soc Rev

REVIEW ARTICLE

View Article Online
View Journal | View Issue

Published on 05 October 2016. Downloaded by Xiamen University on 23/11/2017 07:01:38.

Cite this: *Chem. Soc. Rev.*, 2016, 45, 6742

Tuning two-dimensional nanomaterials by intercalation: materials, properties and applications

Jiayu Wan,[a] Steven D. Lacey,[a] Jiaqi Dai,[a] Wenzhong Bao,*[b] Michael S. Fuhrer*[c] and Liangbing Hu*[a]

Received 8th October 2015

DOI: 10.1039/c5cs00758e

www.rsc.org/chemsocrev

2D materials have attracted tremendous attention due to their unique physical and chemical properties since the discovery of graphene. Despite these intrinsic properties, various modification methods have been applied to 2D materials that yield even more exciting results in terms of tunable properties and device performance. Among all modification methods, intercalation of 2D materials has emerged as a particularly powerful tool: it provides the highest possible doping level and is capable of (ir)reversibly changing the phase of the material. Intercalated 2D materials exhibit extraordinary electrical transport as well as optical, thermal, magnetic, and catalytic properties, which are advantageous for optoelectronics, superconductors, thermoelectronics, catalysis and energy storage applications. The recent progress on host 2D materials, various intercalation species, and intercalation methods, as well as tunable properties and potential applications enabled by intercalation, are comprehensively reviewed.

1. Introduction

Since the successful exfoliation of monolayer graphene, atomic-layer-thick 2D materials have attracted tremendous attention due to their extraordinary physical and chemical properties.[1–5] The novel properties of 2D materials spur fundamental studies and technological advancements for a wide range of applications including (opto)electronics,[6–9] superconductors,[10] photonics,[11] catalysis,[12–18] piezoelectric devices[19] as well as energy storage[20–24] and conversion devices.[25] Despite the unique intrinsic properties of 2D materials, various modification methods have been applied to these materials that yield even more exciting outcomes. We summarize the common modification methods of 2D materials in the following categories: (1) dimensional sizing,[26–28] (2) vertical/lateral heterojunctions,[29,30] (3) alloying and hybridization,[31,32] (4) intercalation,[33–37] (5) external field tuning,[38,39] (6) stacking order,[40] (7) strain engineering,[41] among others. Each of these categories provide unique perspectives and advantages in studying both the fundamental science as well as applications

[a] *Department of Materials Science and Engineering, University of Maryland, College Park, MD 20742, USA. E-mail: binghu@umd.edu*
[b] *State Key Laboratory of ASIC and System, Department of Microelectronics, Fudan University, Shanghai 200433, China. E-mail: baowz@fudan.edu.cn*
[c] *School of Physics, Monash University, Victoria 3800, Australia. E-mail: michael.fuhrer@monash.edu*

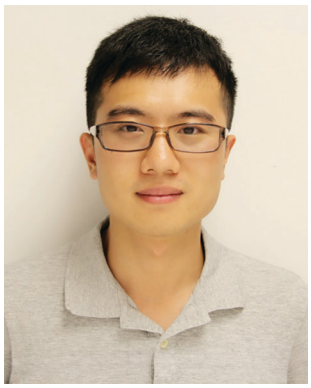

Jiayu Wan

Jiayu Wan received his PhD from Department of Materials Science and Engineering at the University of Maryland, College Park in 2016 and BS from Huazhong University of Science and Technology, China in 2011. His research interests including 2D materials and other nanostructured materials, as well as their applications in opto-electronics, energy storage and flexible electronics.

Steven D. Lacey

Steven Lacey is a PhD candidate in the Department of Materials Science and Engineering at the University of Maryland, College Park and a recipient of the 2015 NDSEG Fellowship. His research focuses on the synthesis, modification, and (in situ) characterization of two-dimensional materials for energy applications beyond lithium-ion batteries.

This journal is © The Royal Society of Chemistry 2016

Published on 05 October 2016. Downloaded by Xiamen University on 23/11/2017 07:01:38.

of 2D materials. For example, dimensional sizing of molybdenum disulfide (MoS_2) from few layers to a monolayer alters the material's band structure from an indirect to a direct band gap,[42] which drastically improves its performance for optoelectronic devices. The narrowing of width also opens up a band gap in graphene.[26] Since many 2D materials without dangling bonds are stable in air and can be placed on arbitrary substrates, heterostructures of 2D materials are possible when different 2D materials are stacked together. Thus, rationally designed 2D vertical structures provide a new degree of freedom for novel band engineering methods and applications.

The intercalation of 2D materials is a process of inserting foreign species in-between the material's large van der Waals gap. Although intercalation of layered materials in their bulk form has been extensively investigated,[43–49] the advent of 2D materials has significantly renewed interest in the field. As long as more than one atomically thin layer is present, intercalation is a possibility. Recent studies demonstrate that the intercalation of nanoscale-thickness layered materials differ greatly compared to intercalated bulk layered materials, and in many cases the differences can result in drastically improved device performance for a wide range of applications.[33,37,50–52] In this review, we will refer to these nanoscale-thickness layered materials as "2D materials" for simplicity, with the assumption that the thickness of the material is much less than its lateral dimensions. Typically the nanometer scale (1–100 nm) is the range in which confinement of electrons and phonons begins to alter the material's electrical, optical, mechanical, and other properties. In this regime, the material begins to be "two-dimensional." To differentiate 2D materials before and after intercalation, we denote "intercalated two-dimensional materials" as "i2DMs" throughout this review.

Among all modification methods, intercalation stands out as a unique avenue to tune the properties of 2D materials for

Jiaqi Dai

Jiaqi Dai received his BS degree in Materials Science and Engineering from Harbin Institute of Technology (2013), China. He is currently a PhD candidate in materials engineering under the supervision of Prof. Liangbing Hu at University of Maryland, College Park, USA. His research mainly focuses on nanotechnologies, advanced solid state energy storage devices, and scientific visualizations.

Wenzhong Bao

Wenzhong Bao is currently a full professor in the School of Microelectronics at Fudan University. He graduated from Nanjing University with a BS in physics (2006). He received his PhD from the University of California, Riverside in 2011, having studied in the Department of Physics and Astronomy. He then worked as a postdoc at the University of Maryland College Park (2012–2015), and the King Abdullah University of Science and Technology (2015). His current research is on two-dimensional layered materials, energy storage and flexible electronics.

Michael S. Fuhrer

Michael S. Fuhrer is a Professor in the School of Physics and Astronomy at Monash University, an Australian Research Council Laureate Fellow, and directs the Monash Centre for Atomically Thin Materials. Fuhrer received his PhD in physics from the University of California, Berkeley in 1998. Prior to his current position, he directed the Center for Nanophysics and Advanced Materials at the University of Maryland. Fuhrer studies the electronic properties of low-dimensional materials, such as carbon nanotubes, graphene, and topological surface states. He is a fellow of the American Physical Society and the American Association for the Advancement of Science.

Liangbing Hu

Liangbing Hu received his BS in applied physics from the University of Science and Technology of China (USTC) in 2002. He did his PhD with Prof. George Gruner at UCLA, focusing on carbon nanotube based nanoelectronics. In 2006, he joined Unidym Inc as a co-founding scientist and worked on printed carbon nanotube transparent electrodes and device integrations. He did his postdoc with Prof. Yi Cui at Stanford University from 2009–2011. Currently, he is an associate professor at University of Maryland College Park. His research interests include nanomaterials and nanostructures, flexible and printed electronics, energy storage and conversion, and roll-to-roll nanomanufacturing.

Published on 05 October 2016. Downloaded by Xiamen University on 23/11/2017 07:01:38.

the following six reasons: (1) intercalation provides the highest possible doping and/or phase change to the pristine 2D materials, especially for few-layer 2D materials; (2) the intercalation process, and the concomitant changes in the properties of 2D materials, is typically reversible; (3) intercalation is controllable, for example by electrochemical voltage, where the concentration of the intercalation species is tunable over a wide range; (4) changes in i2DMs during material preparation can be monitored *in situ* and in real time; (5) intercalation can induce structural changes, such as lattice expansion or even phase changes, for improved or novel physical and chemical properties; (6) the intercalation method adds a new degree of freedom for tuning 2D materials, which can be combined with other modification methods.

Fig. 1 provides a schematic outlook of the field of i2DMs. Starting from the center of the circle, the schematic shows the foreign species that can intercalate within the van der Waals gap of a few-layer 2D material. The intercalants vary from ions, inorganic molecules, organic molecules and metal atoms, as shown in the pink annulus. These intercalants can insert into a variety of (conductive or insulating) host 2D materials through different intercalation methods. After intercalation, many intercalation compounds exhibit outstanding properties that outperform the initial 2D host, which enables high performance optoelectronic, energy and electronic devices, among others. In this review, we will discuss the recent advances of i2DMs, their preparation methods, physical and chemical properties as well as their applications. Insights into the challenges and future opportunities of i2DMs and their potential applications will also be discussed.

2. Materials preparation

2.1 Preparation of 2D materials

To date, single- and multi-layer 2D materials have been prepared using numerous mechanical, chemical and electrochemical methods, which has been summarized by previous works.[2,9,58] Since the focus of this review is on i2DMs, we will briefly introduce common methods for preparing 2D materials, followed by discussion on the intercalation of 2D materials obtained from these methods. Note that specific preparation methods for i2DMs will be discussed later in this review.

Mechanical exfoliation. In general, bulk versions of 2D materials are layered structures held together by strong in-plane covalent bonds and weak out-of-plane van der Waals forces. Exfoliation of these layered materials is enabled by taking advantage of their weak interlayer forces. Since Novoselov *et al.* successfully exfoliated bulk layered crystals into atomically thin layers (2D materials), the mechanical exfoliation (or scotch tape method) has gained widespread use to fabricate 2D materials as well as unique planar devices.[55,59,60] This method was originally developed for exfoliating 2D graphene but has been universally applied to other 2D materials including hexagonal boron nitride (hBN) as well as numerous 2D transition metal dichalcogenides,

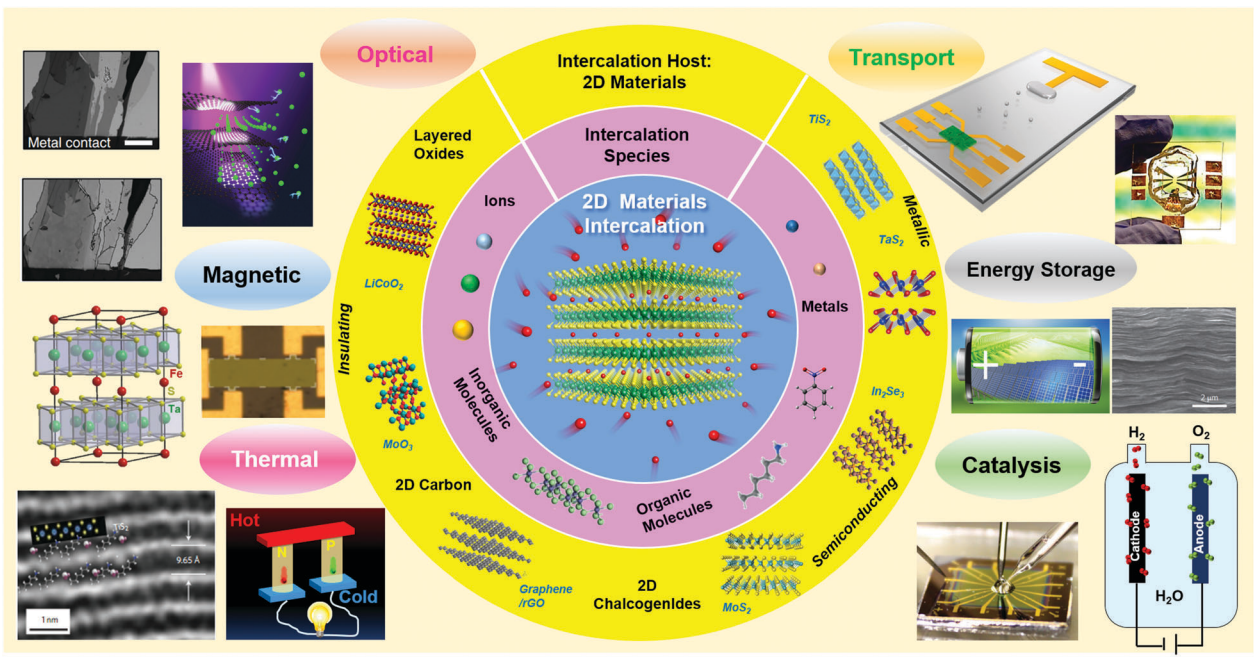

Fig. 1 Schematic of tunable intercalation of 2D materials. Summary of the intercalation species, intercalation host (*i.e.* 2D materials), properties, and applications of i2DMs.[37,52–57] Reproduced with permission from ref. 37. Copyright 2014, Nature Publishing Group. Reproduced with permission from ref. 52. Copyright 2007, American Physical Society. Reproduced with permission from ref. 53. Copyright 2014, American Chemical Society. Reproduced with permission from ref. 54. Copyright 2015, Nature Publishing Group. Reproduced with permission from ref. 55. Copyright 2015, John Wiley and Sons. Reproduced with permission from ref. 56. Copyright 2016, Nature Publishing Group. Reproduced with permission from ref. 57. Copyright 2016, Nature Publishing Group.

 This journal is © The Royal Society of Chemistry 2016

Published on 05 October 2016. Downloaded by Xiamen University on 23/11/2017 07:01:38.

among others.[58] Mechanically exfoliated 2D materials are excellent candidates for fundamental studies due to non-contaminated basal planes. Thus, these "clean" 2D materials are useful for current i2DM investigations. Unfortunately, the material yield from this method is insufficient for large-scale production.[61]

Chemical vapor deposition (CVD). CVD is a well-known bottom-up growth technique for 2D materials (graphene, MoS_2, boron nitride, among others) providing large-scale synthesis of 2D materials with precisely controlled layer numbers.[62–70] In this growth process, the deposition of solid materials occurs *via* chemical reactions of the precursor species which are controlled through different processing parameters.[62–64,71] 2D materials prepared by CVD enable the scalable production of i2DMs. However, transfer methods (such as the poly(methyl methacrylate) method) may be needed to relocate the 2D materials to the substrate of choice.[62,72–74] Structural defects and polymeric residue are often introduced during the growth and transfer processes which alter the material's properties.

Liquid-based exfoliation. An alternative approach to obtain large scale production of 2D materials is through chemical methods *via* liquid-based exfoliation.[64,75–85] Some liquid-phase exfoliation methods rely on intercalation chemistry where foreign species (solvent molecules, chemically or electrochemically induced intercalants) are inserted into the van der Waals gap of each layer. The insertion of guest species increases the interlayer spacing, weakens the adhesion between layers and facilitates separation into 2D nanosheets. Other liquid phase exfoliation methods chemically modify the layered material, reduce the van der Waals forces between layers and then begin to exfoliate.[86,87] To initiate the intercalation and exfoliation of 2D materials, sonication and centrifugation techniques are conventionally employed. However, sonication breaks the layers into sheets with small lateral dimensions (typically <5 μm, although graphene oxide flakes can be as large as 100 μm) and creates mainly few-layer 2D materials.[75,79,88] The 2D material solution acts as an "ink" that can be printed into large and uniform networks, which enables scalable i2DM production.

Many other growth methods exist for certain types of 2D materials including carbon segregation (*e.g.* growth of graphene on SiC) and chemical synthesis.[4,9,89] Few-layer graphene grown by the carbon segregation method are also suitable for intercalation processes.[90] Synthetic methods such as 2D-templated synthesis and hydro/solvothermal synthesis are widely applied to obtain 2D materials.[91] However, most 2D materials synthesized with these methods are non-layered 2D materials and do not fall within the scope of i2DMs.

2.2 Intercalation of 2D materials

A number of methods have been adopted (from intercalation in bulk layered materials) and developed to obtain functional i2DMs. In this section, we will emphasize two common groups of i2DM preparation methods: chemical intercalation and electrochemical intercalation. Each of these methods can be further divided into two categories. Depending on where the intercalation species originates, chemical intercalation can be classified as gas phase intercalation (chemical vapor transport methods) and liquid phase intercalation (wet chemical methods). Electrochemical intercalation is divided into liquid electrolyte intercalation and solid-state electrolyte intercalation. Other less common methods for 2D materials such as molten metal (salt) intercalation (*e.g.* Li in few-layer graphene), solid state chemical intercalation and co-intercalation techniques will not be discussed in this i2DM review.[43,92] Table 1 compares and summarizes each intercalation method discussed in the following subsections.

Chemical vapor transport methods. A wide range of materials, including metals and inorganic molecules can be intercalated into 2D materials through chemical vapor-phase reactions. The most common preparation procedure is the two-zone vapor transport method where at high vacuum, both the intercalant (such as metal chlorides and other diatomic molecules) and host materials (such as few-layer graphene, MoS_2, among others) are heated at different temperatures and the gradient between them enables well-controlled intercalation stages. The intercalation process largely depends on the size of samples. For example, large, thick samples often intercalate slower and less homogeneously compare to small, thin flakes. Several groups have demonstrated enhanced electrical, optical and magnetic properties by intercalating few-layer graphene with ferric chloride ($FeCl_3$) for use in novel optoelectronic devices.[52,93]

Wet-chemical methods. Wet-chemical methods refer to the intercalation process that occurs through solution-based non-electrochemical reactions. Specific precursors in solution(s) are added to 2D material(s) to facilitate the intercalation process. For example, Li-intercalated tungsten disulfide (WS_2) can be achieved by mixing the 2D material (WS_2) with *n*-butyl lithium in a hexane solution.[94] Zerovalent intercalation relies on solution-based reactions to insert zerovalent metal species within the van der Waals gap of 2D materials.[95–97] In this way, numerous zerovalent metals including Cu, Ag, Au, Co, Fe, In, Ni, Pd and Sn can be intercalated into 2D materials such as bismuth selenide (Bi_2Se_3) and modify its physical and chemical properties.[96] Zerovalent intercalation also facilitates the formation of large stoichiometry intercalation compounds, which are rarely achieved with other intercalation methods. Unlike electrochemical intercalation, chemical intercalation methods can intercalate non-conductive host materials such as boron nitride.[98]

Electrochemical methods. Electrochemical methods enable the intercalation of cations (such as Li-ion) or anions (such as PF_6^- ions) in the interlayer spacing of 2D materials (such as few-layer graphene) through electrochemical reactions.[99,100] These electrochemical approaches typically rely on a test cell configuration where the metal ions are supplied by the reference metal (*e.g.* Li) anode and intercalate into the 2D material cathode through the ionically conducting liquid/solid-state electrolyte through an external bias. In liquid electrolyte, the ion moves faster than in a solid electrolyte and the voltage profile of intercalation compounds are well defined. However, a liquid electrolyte could yield unclean intercalation compounds due to the formation of a solid electrolyte interphase (SEI) upon cycling. Devices with liquid electrolyte are also more difficult to fabricate than solid electrolyte devices due to solvent/salt instability and device encapsulation. Unlike chemical methods,

Published on 05 October 2016. Downloaded by Xiamen University on 23/11/2017 07:01:38.

Table 1 Comparison of common intercalation methods

Methods		Brief description	Advantages	Disadvantages
Chemical intercalation	Chemical vapor transport (gas phase)	In high vacuum, the intercalant and host materials are heated at different temperatures. The temperature gradient between them controls the formation of staged intercalation compounds.	• Scalable • Available for many intercalants • Available for all most 2D materials (including non-conductive ones) • Product without contamination	• Slow kinetics • Vacuum process required • High temperature • Irreversible • Low controllability • Hard to achieve real time characterization
	Wet-chemical methods (liquid phase)	2D materials soaked in solution(s) with the desired precursor/solvent. The intercalation process takes place through chemical reactions.	• Reversible • Scalable • Clean product (no SEI) • Enable organic matter intercalation • Allow high degree of intercalation • Available for all host 2D materials (include non-conductive ones)	• Hard to achieve real time characterization • Hard to precisely control the concentration of intercalants • May result in swelling of host 2D material bundles • Slow kinetics
Electrochemical intercalation	Liquid electrolyte	In a liquid electrolyte, the host 2D material (cathode) is intercalated. The intercalation process is controlled by an external bias between the two electrodes. Ions from the liquid electrolyte intercalate between the 2D layers.	• Scalable • Reversible • High controllability • Fast kinetics • Real time/*in situ* characterization	• Sometimes unclean product (with SEI) • Only available for certain intercalants • Host 2D materials need to be conductive • May result in swelling of host 2D material bundles
	Solid electrolyte	In a solid electrolyte, the host 2D material (cathode) is intercalated. The intercalation process is controlled by an external bias between the two electrodes. Ions from the solid electrolyte intercalate between the 2D layers.	• Reversible • Medium temperature • High controllability • Real time/*in situ* characterization • Clean product	• Slow kinetics • Limit to micro/nano scale studies • Only available for certain intercalants • Host 2D materials need to be conductive

electrochemical intercalation can be controlled to precise doping levels based on the applied electrochemical voltage. The specific concentration of intercalated species tunes material properties enabling in-depth experimental studies and potential advancements in the field of 2D materials. A rational design of electrochemical intercalation platforms can lead to both fundamental studies and the scalable production of i2DMs.

3. Characterization of i2DMs

The intrinsic properties of 2D materials can be greatly modified by intercalating foreign species. The nature of the intercalants (*i.e.* intercalant size, charge, *etc.*) as well as the structural stability, composition and dimensions of the 2D materials drastically influences its physical and chemical properties and expands the potential applications of this new class of (intercalated) 2D materials. More specifically, 2D materials can exhibit extraordinary electrical transport as well as optical, optoelectronic, magnetic, catalytic and electrochemical properties, which will be discussed in more detail later in this review. To understand and investigate these intriguing properties, the i2DMs require characterization on a material and device level.

In situ and real time characterization techniques offer unique insight into intercalation mechanisms and a material's properties. Bao *et al.* simultaneously studied the electrical transport and optical properties of Li-intercalated graphite in real time using a unique planar nanobattery configuration (Fig. 2a–c).[37] The *in situ* investigations are enabled by the planar battery platform where few-layer graphene sheets are mechanically exfoliated and placed on a glass substrate. To create electrical connections, copper is evaporated into specific patterns using a previously described shadow mask technique.[101] Since a liquid electrolyte and Li metal reference are required for electrochemical Li intercalation, the device has to be fabricated in an Ar-filled glove box and sealed with a piece of glass and polydimethylsiloxane (PDMS). Note that the intercalation process causes the interlayer spacing of the graphene layers to steadily increase, which induces strain in the 2D material as well as cracks the electrical connections. To alleviate this issue, the copper connections were deposited prior to the transfer of mechanically exfoliated 2D materials (Fig. 2a–c). Fig. 2d depicts the set-up used to measure electrical transport and the optical properties by coupling an electrochemical battery tester with a transmission optical microscope.[55] Direct observation of the intercalation process and Li staging in graphite is quantified by matching the changes in optical transmittance to the measured voltage of the planar nanobattery.[37] Additional *in situ* studies can be conducted using planar battery devices and scanning probe techniques such as *in situ* atomic force microscopy (AFM).[102] Fig. 2e is a schematic of a planar battery used to study the real-time topographical evolution of 2D materials such as MoS_2 during Na (de)insertion in an open liquid electrochemical cell under dry conditions ($T \sim 20$ °C; $T_{dew} \sim -40$ °C).[60] Electrochemical intercalation can be conducted with solid polymer or gel electrolytes (*i.e.* polyethylene oxide and a Li salt) rather than liquid electrolytes where a gating bias controllably intercalates

 This journal is © The Royal Society of Chemistry 2016

Published on 05 October 2016. Downloaded by Xiamen University on 23/11/2017 07:01:38.

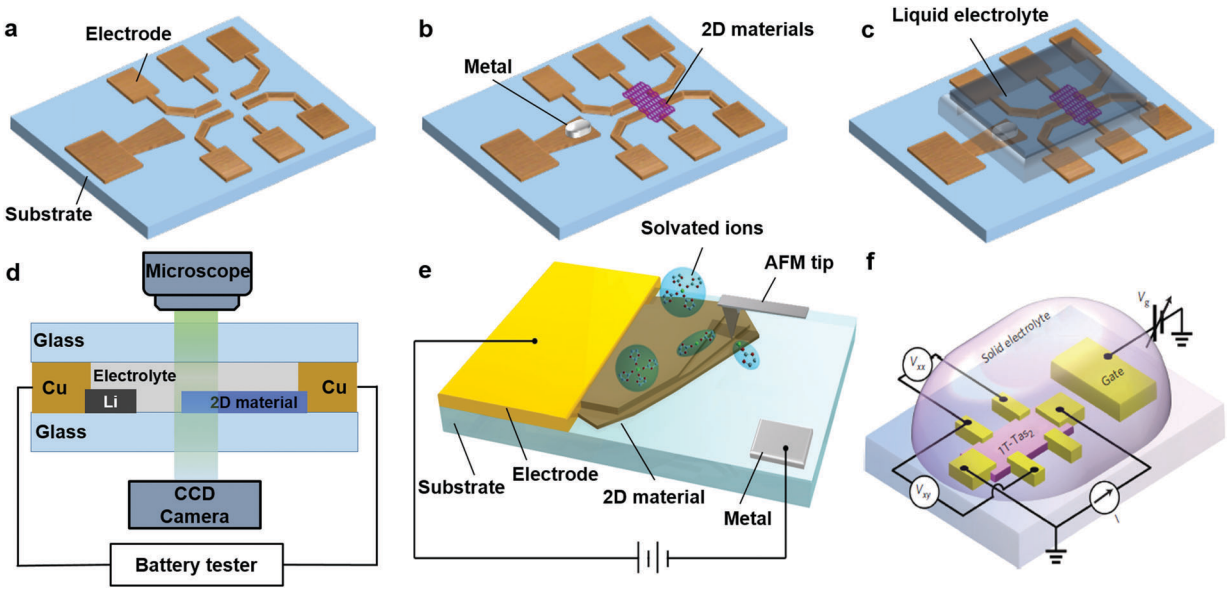

Fig. 2 Devices for the intercalation of 2D materials (a–c) fabrication process schematic for *in situ* optoelectronic and electrical transport measurements using a planar nanobattery device.[37] Reproduced with permission from ref. 37. Copyright 2014, Nature Publishing Group. (d) Schematic of *in situ* optical and electrochemical measurements for i2DM devices (with a transparent substrate) where an electrochemical battery tester and optical microscope are integrated.[55] Reproduced with permission from ref. 55. Copyright 2015, John Wiley and Sons. (e) Schematic of *in situ* AFM measurements for 2D material intercalation in liquid electrolyte.[60] Reproduced with permission from ref. 60. Copyright 2014, American Chemical Society (f) Schematic structure of a TaS_2 ionic field-effect transistor (iFET) with a solid gel electrolyte. The set-up enabled gate-controlled intercalation of Li.[33] Reproduced with permission from ref. 33. Copyright 2015, Nature Publishing Group.

Li and dopes 2D materials to high levels. An ionic field-effect transistor can electron dope atomic layers in a similar manner to the charging process in LIBs (Fig. 2f). To create this device, tantalum disulfide (TaS_2) flakes are exfoliated onto a glass substrate and gold electrodes are deposited *via* e-beam lithography. A solid electrolyte is placed in contact with the device components and acts as a medium to facilitate gate-controlled intercalation.

Unique 2D devices enable *in situ* optoelectronic and transport measurements. Fig. 3a exhibits the reversible changes in transmittance in the visible range at different stages of Li-intercalated graphite using a planar nanobattery device. Bao *et al.* determined that there is a simultaneous increase in conductivity and optical transmittance for thin lithiated graphite sheets which is dependent on sheet thickness and the amount of Li intercalated. The process is highly reversible and the *in situ* methodology used to investigate the electrical resistance, optical transmission and nanoscale structure upon lithiation can be adopted for investigation of other energy storage or electronic materials.[37] Wan *et al.* studied the lithiation of MoS_2 crystals using a similar approach in terms of *in situ* investigations and device fabrication.[55] Lithiated MoS_2 exhibited simultaneous increases in both conductivity and transmittance which opposes the conventional (inverse) relationship between these material properties. Additionally, a new rapid charging strategy became possible due to the proposed Mo nanoparticle conductive network which significantly increased cell capacity.[55] Details of these studies are described in the following sections.

Optical studies including Raman spectroscopy as well as other *in situ* techniques (*i.e. in situ* TEM and *in situ* AFM) are possible using the planar battery configuration.[55,60] As shown in Fig. 3b, the planar battery on a glass substrate enables Raman spectra to be taken before, during and after Li-intercalation. Noticeable changes in the Raman spectra are observed confirming the potential of this characterization technique for differentiating ion-intercalation stages in 2D materials. Earlier work on *in situ* Raman spectroscopy of Li-intercalated bulk graphite can be found decades ago.[103] Zhao *et al.* monitored the intercalation of ferric chloride ($FeCl_3$) in cleaved few-layer graphene by Raman spectroscopy and estimated the Fermi level by the intensity of the 2D and G peaks.[104] Raman mapping of i2DMs also yields enhanced visibility and contrast for intercalated areas with different flake thicknesses. Fig. 3c exhibits an optical image of mechanically exfoliated graphene flakes before $FeCl_3$ intercalation and the contrast spectra afterwards. For ion-intercalation to occur in 2D materials, at least two layers are required to accommodate the foreign species within the van der Waals gap.[105] In $FeCl_3$-intercalated graphitic materials, the amount the G peak blue shifts is dependent on the number of layers (shift decreases with increase in layer thickness) as well as the level of doping. The layer thickness as well as the differences in band shape can be identified based on the 2D peak. Zhan *et al.* used Raman spectroscopy and mapping to prove that the few-layer graphene was fully and uniformly intercalated with $FeCl_3$ (Fig. 3c).[105] During the intercalation process, graphene's electronic band structure and properties were modified due to strong charge transfer doping.

AFM is a conventional characterization technique to determine the thickness and morphology of 2D materials. However, this nanoscale resolution scanning probe microscopy technique can be coupled with an electrochemical workstation (often referred

Published on 05 October 2016. Downloaded by Xiamen University on 23/11/2017 07:01:38.

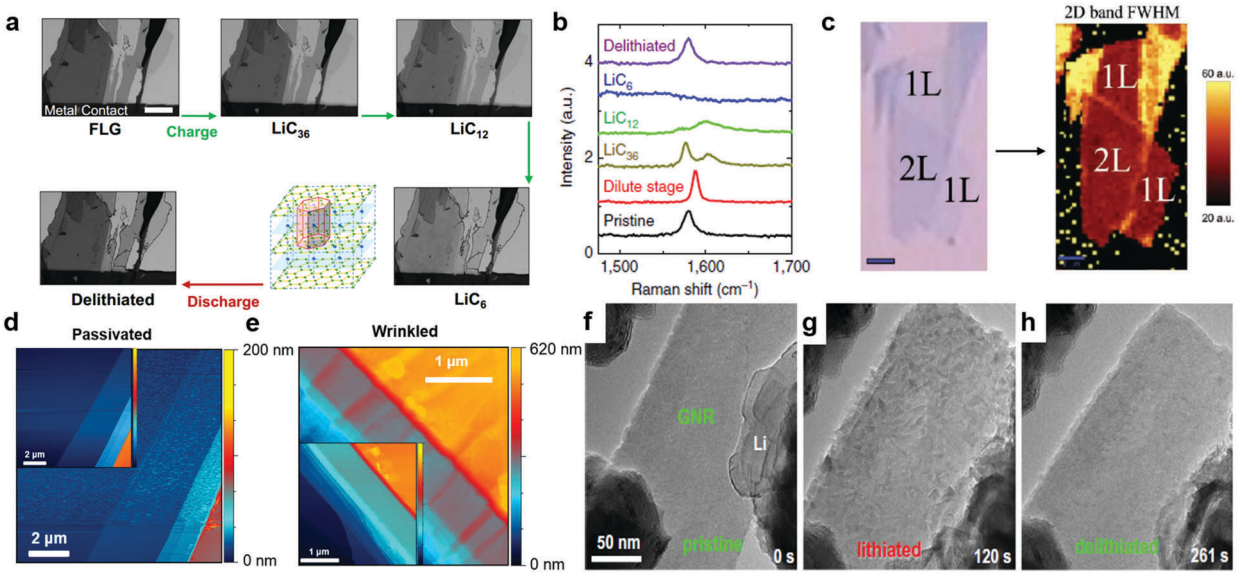

Fig. 3 Characterization of i2DMs (a) transmission optical microscope images of ultrathin graphite at different Li-intercalation stages.[37] (b) Raman spectra of Li-intercalated ultrathin graphite at different Li-intercalation stages.[37] Reproduced with permission from ref. 37. Copyright 2014, Nature Publishing Group. (c) Optical image and Raman image of bilayer and monolayer graphene before and after $FeCl_3$ intercalation respectively. The uniform linewidth across the bilayer region indicates homogeneous intercalation of $FeCl_3$.[105] Reproduced with permission from ref. 105. Copyright 2010, John Wiley and Sons. *In situ* AFM images of (d) SEI passivation [OCV to 1.0 V] and (e) wrinkled MoS_2 flakes [OCV to 0.4 V] due to Na-intercalation. The insets are AFM images before passivation or wrinkling occurs.[60] Reproduced with permission from ref. 60. Copyright 2014, American Chemical Society (f–h) morphological evolution of a (de)lithiated GNR using *in situ* TEM.[110] Reproduced with permission from ref. 110. Copyright 2012, Elsevier.

to as electrochemical AFM or EC-AFM) to successfully intercalate 2D materials through an applied bias. Siegenthaler and coworkers determined the step height changes of Li-intercalated HOPG *via in situ* AFM for the first time.[106] The experiments were conducted using a homemade electrochemical cell in a laminar flow glovebox and demonstrated step height changes of ~17% in a conventional liquid electrolyte.[106] *In situ* AFM studies also yield information about the failure mechanisms of intercalated layered materials and 2D materials. Alliata *et al.* obtained the expansion of HOPG due to anion intercalation in acidic solutions.[107] Blistering of the HOPG layers was observed as well as increases (14–32%) in the graphene interlayer distances depending on the amount of graphene layers present in the experimental setup.[107] *In situ* AFM experiments of Li-intercalated HOPG also demonstrate structural degradation. As the potential decreases from OCV to 0.005 V *vs.* Li/Li^+, the basal planes of Li-intercalated HOPG begin to distort and form line-like features across the graphene planes.[108] If a low potential is held for extended periods of time, cracking of the graphene is induced.[108] Beyond *in situ* graphene studies, Lacey *et al.* created a planar battery with mechanically exfoliated MoS_2 flakes, copper electrical connections, and a Na metal reference electrode and investigated the structural and topographical changes upon sodiation using *in situ* AFM in an open liquid electrochemical cell.[60] *In situ* AFM was conducted in a dry room environment (T ~ 20 °C; T_{dew} ~ −40 °C) to reduce oxidation of the Na metal and enable an open cell configuration.[60] Fig. 3d depicts the formation of a ~20 nm passivation layer (*i.e.* solid electrolyte interphase or SEI) on the MoS_2 flakes, which started around 1.5 V.[60] During electrochemical testing and continuous scanning of the AFM tip, the soft polymeric portion of the SEI can be removed leaving the hard salt-like portion behind. Permanent structural wrinkling along the flake plateaus is observed as the potential reaches 0.4 V and 1.1 Na ions are inserted (Fig. 3e). The structural wrinkling of the MoS_2 flakes coincides with the previously proposed reaction mechanism.[109]

Since the intercalation of 2D materials causes structural/volume changes, *in situ* TEM techniques are advantageous for structural identification and can yield much insight into the electrochemical insertion process. To verify the charge rate dependence of the proposed Mo nanoparticle conductive network in lithiated MoS_2, *in situ* electrochemical TEM experiments were employed.[55] Liu *et al.* glued graphene nanoribbons to an aluminum rod and used the grown Li_2O layer on the Li/tungsten rod as the solid electrolyte for *in situ* TEM.[110] The structural evolution of graphene nanoribbons can be investigated during the lithiation and delithiation processes.[110] Fig. 3f–h shows the graphene nanoribbon before lithiation, during Li insertion and after delithiation, respectively.[110] The lithiation/delithiation processes were reversible and the graphene nanoribbons accommodated the strains associated with Li insertion easily. In this case, the graphene materials, which were synthesized by splitting carbon nanotubes, have potential as mechanically robust and durable LIB electrodes. Similarly, Wan *et al.* used a Li metal electrode on a tungsten rod and a MoS_2 electrode on a gold rod attached to a TEM-STM holder for *in situ* TEM observations as well as the identification of the material's crystal structure by diffraction.[55] Other characterization techniques such as scanning tunneling microscopy (STM) and angle-resolved photoemission spectroscopy (ARPES) have also been used to investigate i2DMs.[111]

 This journal is © The Royal Society of Chemistry 2016

Published on 05 October 2016. Downloaded by Xiamen University on 23/11/2017 07:01:38.

4. Tuning electronic properties by intercalation

Previous electrical transport studies which focused on the intercalation of bulk layered materials have been recently revisited using their atomically-thin counterparts: 2D materials.[33,37,54,93,105] Since intercalated species tend to induce charge transfer in the host 2D materials (although charge transfer does not occur in all cases),[112,113] the Fermi energy is shifted and the density of energy states at the Fermi level increases. Subsequently, this increases the charge carrier density of the 2D materials. Note that the doping capability is far beyond conventional electric-field-induced doping levels in film-based devices[38,39] or through electron-double-layer (EDL) surface gating[114–116] with an ionic liquid (Table 2). In general, intercalated compounds are more chemically robust than compounds with physically/chemically adsorbed molecules on the surface. This is due to the chemically inert, impermeable atomically thick 2D layers that protect and encapsulate the unstable intercalants.

Table 2 Maximum (max) carrier density of 2D materials with different doping methods

Doping method	Max carrier density (n_{2D}[a])	Ref.
Electric field gating	5×10^{12} cm^{-2}	38 and 39
Ionic liquid	0.2×10^{15} cm^{-2}	114 and 115
Polyatomic intercalation ($FeCl_3$)	$(0.3–0.9) \times 10^{15}$ cm^{-2}	93
Monoatomic intercalation (Li, Na, K)	$(0.1–1) \times 10^{15}$ cm^{-2}	37 and 115

[a] n_{2D} is defined as the carrier density per layer.

An early experimental study of electrical transport in i2DMs was reported by Kim *et al.*[117] where ferric chloride $(FeCl_3)_n$ was intercalated into bilayer graphene (BLG) using a two-zone chemical vapor transport method to achieve a vapor-phase reaction of $FeCl_3$ and BLG. By patterning the BLG sheet to a Hall-bar geometry (Fig. 4a inset), the local intercalation structure can be extracted by analyzing Shubnikov–de Haas oscillations (SdHO) (Fig. 4a), represented as the longitudinal resistance (R_{xx}) *vs.* perpendicular magnetic field, B, at different temperatures. At low temperatures, $R_{xx}(B)$ oscillates with two distinct frequencies, which arise from two different carrier densities associated with the intercalated bilayer (decoupled to two separate monolayers) and the unintercalated bilayer (coupled). Fig. 4b represents the spatially inhomogeneous intercalation of $FeCl_3$, with an intercalated domain size much smaller than 500 nm across the entire sample. Additionally, the band diagrams of the two domains

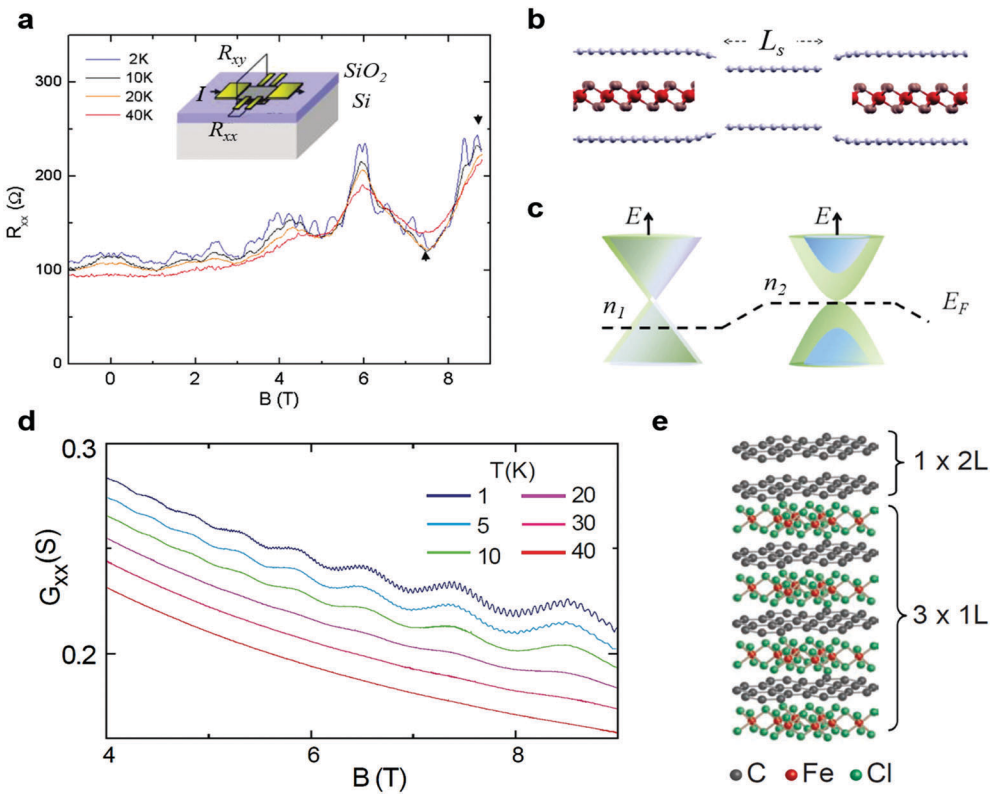

Fig. 4 Electrical properties of $FeCl_3$-intercalated few-layer graphene (a) SdH oscillations in $R_{xx}(B)$ are recorded at temperatures of 2, 10, 20, and 40 K. Inset shows a schematic of an intercalated bilayer graphene device.[117] (b) Atomic structural model of intercalated and unintercalated bilayer graphene domains.[117] (c) Band diagrams of two domains exhibiting different electronic properties, especially chemical potential, carrier density, and band structures.[117] Reproduced with permission from ref. 117. Copyright 2011, American Chemical Society. (d) Longitudinal conductance as a function of magnetic field at different temperatures (curves shifted for clarity). (e) Schematic crystal structure of a 5L $FeCl_3$-intercalated graphene in which the detailed structure was determined by electrical transport measurements.[93] Reproduced with permission from ref. 93. Copyright 2012, John Wiley and Sons.

Published on 05 October 2016. Downloaded by Xiamen University on 23/11/2017 07:01:38.

exhibit different electronic properties as shown in Fig. 4c. A similar work[93] was later reported by Khrapach *et al.*, using an exfoliated five layer (5L) graphene device. At low temperatures, SdHO also exhibits two distinct types of periodic magneto-oscillations (Fig. 4d), with further analysis indicating the presence of four parallel hole gases: one with unintercalated bilayer character and three with monolayer character (Fig. 4e).

Beyond $FeCl_3$ intercalation, metal intercalation in few-layer graphene has also been investigated. Metal intercalation in bulk graphite has been shown to induce superconductivity,[43,118,119] and recently, abnormal superconducting behavior of metal decorated graphene in the 2D limit has also been suggested.[120] Thus, it is crucial to prepare and characterize the electronic properties of metal intercalated few-layer graphene. Kanetani *et al.*, prepared Li- and Ca-intercalated bilayer graphene (denoted as C_6LiC_6 and C_6CaC_6, respectively) under ultrahigh vacuum and studied their electronic bandstructures with ARPES.[111] Fig. 5a exhibits a typical STM image of successfully prepared C_6CaC_6. Note that the positions of the Ca atoms within the bilayer graphene's honeycomb structure are marked by purple dots. The electronic bandstructure of C_6CaC_6 was calculated (Fig. 5b) and experimentally measured (Fig. 5c and d). When metal intercalants electron dope the material, there is an upshift of the Fermi energy (C_6CaC_6 is $\sim$1.8 eV and C_6LiC_6 is $\sim$1.5 eV). The computation and experimental results agree well, which shows that C_6CaC_6 has a nearly degenerated π^* band as well as an interlayer band (IL). However, the IL is absent in the C_6LiC_6 (Fig. 5e and f). This demonstrates that the IL is not typical for all types of metal intercalated few-layer graphene (Fig. 5e and f). Note that the free-electron-like IL near the E_F seems to be responsible for superconductivity in bulk graphite intercalation compounds. Studies of superconductivity in metal intercalated few-layer graphene are intriguing and should be pursued further.[121]

Bao *et al.* used an *in situ* planar nanobattery setup to investigate the electrical transport of few-layer graphene during controlled electrochemical Li intercalation.[37] Fig. 5g shows the sheet resistance, R_s, of few-layer graphene with different thicknesses both before intercalation as well as at different intercalation states: LiC_{12} and LiC_6. Fully intercalated few-layer graphene samples invariably exhibit a lower resistivity compared to their pristine state.[122] The direct current (DC) sheet conductivity, σ_{dc}, was estimated to be 11 mS per layer in the LiC_6 state, which is approaching the intrinsic limit of conductivity for doped graphene (33 mS per layer) set by electron-acoustic phonon scattering.[122] Furthermore, by probing the Hall resistance $R_{xy}(B)$, the negative slope indicates that electrons are the type of charge carriers for few-layer graphene after Li intercalation (Fig. 5h). Additionally, the carrier density, n_H, can be determined by the Hall coefficient: $R_H = R_{xy}/B$ where R_H is related to n_H by $n_H = 1/eR_H$. The experimental results reveal that the two dimensional carrier density n_{2D} ranges from 1.0×10^{14} to

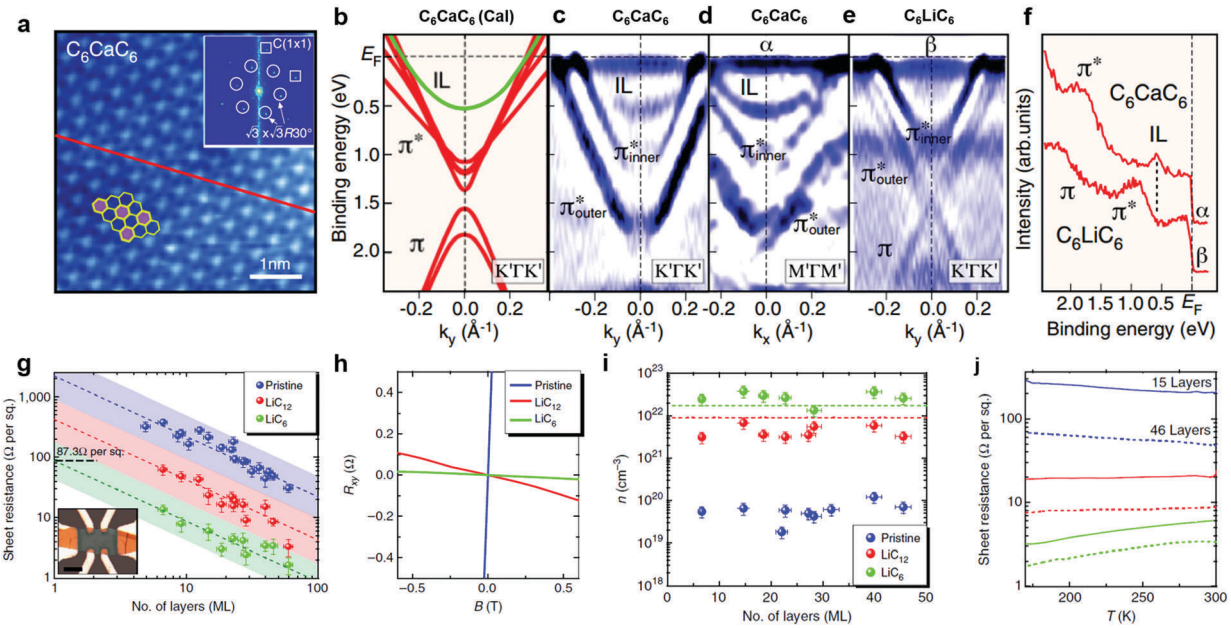

Fig. 5 Electrical properties of metal-intercalated few-layer graphene (a) STM image of C_6CaC_6. The inset shows the Fourier-transform image. (b) The calculated bandstructure of C_6CaC_6 and the experimental band dispersion of (c and d) C_6CaC_6 and (e) C_6LiC_6, which was obtained by taking the second derivative of the ARPES spectra. (f) The ARPES spectra of C_6CaC_6 and C_6LiC_6 at the Γ point.[111] Reproduced with permission from ref. 111. Copyright 2013, National Academy of Sciences, USA. (g) Resistivity *versus* thickness for ultrathin graphite sheets with different thicknesses. Data for pristine (red) and two lithiated stages (LiC_{12} and LiC_6 indicated by green and blue) are shown. Inset shows an optical image of an ultrathin graphite device with Hall-bar geometry before intercalation. (h) Hall resistance of a 4 nm-thick pristine few-layer graphene sheet and its LiC_{12} and LiC_6 states as a function of magnetic field. (i) Carrier density calculated from Hall measurements as a function of ultrathin graphite thickness. (j) Temperature-dependent sheet resistance for two ultrathin graphite samples. Blue, red and green denote pristine, LiC_{12} and LiC_6 stages, respectively.[37] Reproduced with permission from ref. 37. Copyright 2014, Nature Publishing Group.

 This journal is © The Royal Society of Chemistry 2016

Published on 05 October 2016. Downloaded by Xiamen University on 23/11/2017 07:01:38.

2.3×10^{14} cm^{-3} for LiC_{12} and 0.5×10^{15} to 1.2×10^{15} cm^{-2} for LiC_6 (Fig. 5i). Fig. 5j exhibits the temperature dependence on sheet resistance. Note that LiC_{12} exhibits a moderate temperature dependence. $R_s(T)$ is metallic at the LiC_6 state and the pristine sample always exhibits weak non-metallic behavior, which is consistent with previous studies.[123]

Li can also be intercalated into the van der Waals gap of other 2D materials, such as MoS_2 crystals. Using the same *in situ* planar nanobattery setup, Wan *et al.* studied the electrical resistance changes during electrochemical lithiation.[55] As shown in Fig. 6a, the four-probe electrical resistance of a 35 nm-thick MoS_2 crystal was probed simultaneously with sweeping electrochemical potential at a constant lithiation current of 0.5 μA. During the first lithiation cycle, a rapid decrease of the electrochemical potential as well as the resistance occurred in region I, which can be interpreted as a reversible phase change from 2H-MoS_2 to 1T-Li_xMoS_2 induced by lattice distortions during intercalation. At the end of region II, the resistance rises abruptly and remains higher than the initial resistance in region III. This corresponds to the conversion reaction from 1T-$LiMoS_2$ to an insulating matrix formed by Li_2S and Mo metal. A similar work by Xiong *et al.* studied the thickness-resistance dependence of lithiated MoS_2 using the same experimental setup.[124] As shown in Fig. 6b, MoS_2 crystals show a drastic decrease (more than two orders of magnitude) in electrical sheet resistance upon Li intercalation, down to a few nanometers in thickness. Furthermore, the sheet resistance of Li_xMoS_2 devices with different thicknesses decreases more than five times as the potential changes from ~2.3 to 1.2 V *versus* Li/Li$^+$ (Fig. 6c). Note that changing the potential corresponds to tuning the Li concentration in MoS_2.

Due to the phase transition of MoS_2 induced by reversible Li intercalation, Kappera *et al.* developed a methodology to locally convert regions of the semiconductive 2H-MoS_2 nanosheets into metallic 1T-Li_xMoS_2 phases and use them as electrodes to achieve MoS_2 FETs with low contact resistance.[51] In Fig. 6d and e, Au metal pads were contacted to the 1T phase areas, and the contact resistance was extracted using the transfer length method (TLM). In comparison to the typical MoS_2 devices, the resistance of the 1T contacts decreased by a factor of ~5 from 1.1 kΩ μm to 0.2 kΩ μm at zero gate bias. By further tuning the back gate voltage, the contact resistance decreased by another factor of three at a gate bias of +30 V, as shown in the inset of Fig. 6e. Zhang *et al.*, for the first time, demonstrated that potassium (K) intercalation induced a phase change in MoS_2 as well as superconductivity in its intercalation compounds (Fig. 6f). By removing the K intercalants, the superconducting effect of 1T/1T′ structured MoS_2 disappeared. Thus, to maintain superconductivity, it is essential to retain the intercalated K.[125] Fig. 6g displays the "dome-like" superconducting phase induced by intercalation or ionic electrolyte gating. This behavior suggests that the superconductivity of heavily doped 2H-MoS_2 is not simply controlled by changes in the density of states.[115] Note that superconductivity studies of intercalation compounds focus on their bulk forms however, we anticipate more interesting effects with i2DMs.

In addition to MoS_2 crystals, phase transitions also occur in TaS_2 during Li intercalation. Yu *et al.*[33] studied various charge-ordered states in 1T-TaS_2 ionic field-effect transistors (iFETs) with different 2D crystal thickness, in which gate-controlled Li intercalation modulates the phase transition (Fig. 7a). The intercalation-controlled phase transitions can be further probed by measuring the temperature-dependent resistance in samples at various fixed gate voltages (*i.e.* fixed Li concentrations), as shown in Fig. 7b–d. A clear thickness dependence is present for each sample: the 14 nm-thick sample retains all the charge-density wave (CDW) phases; the 8 nm-thick sample is in the quasi-two-dimensional limit, where all but the commensurate CDW (CCDW) phases remain; the 3.5 nm-thick sample is an insulator without any phase transitions. At 10 K under Li intercalation, the 14 nm device spans three different phases and shows resistance changes of five orders of magnitude (Fig. 7e, upper panel). The volumetric charge carrier density, n_{3D}, in the three phases can also be determined from Hall measurements (Fig. 7e, lower panel). More information about the competition, coexistence and cooperation of various collectively ordered states of intercalated TaS_2 are summarized in the phase diagrams shown in Fig. 7f–h.

5. Tuning photonics and optoelectronic properties by intercalation

The unique electronic structure of 2D materials can lead to interactions with photons. For instance, graphene's band structure reveals a linear relation between energy and momentum, known as the Dirac cone. This band structure enables interesting properties such as linear optical absorption with universal optical conductance as well as broadband interband transitions. These properties result in a broad range of applications such as transparent conductors and broadband photodetectors.[126] For group VI transition metal dichalcogenides (TMDs) (such as MoX_2 and WX_2), a change between indirect and direct band gaps would occur as the layer number decreases from multilayer to monolayer. This change leads to a much higher efficiency in the photon absorption process for monolayer TMDs, in which an additional phonon is no longer needed. Thus, applications such as photovoltaics, LEDs and photodetectors are enabled by these 2D materials. The excellent properties and successful scalable production of 2D materials also makes them intriguing for photonic and optoelectronic devices that require flexibility and transparency. In this section, we will review how intercalation tunes the optical properties of 2D materials to improve their performance for potential applications.[6]

Graphene and its derivatives have been extensively studied as transparent electrodes.[25,127] The intrinsically high electron mobility, atomic thickness, and broadband transparency in mono- and few-layer graphene makes it an ideal candidate for transparent conductors. Regardless, the combined performance for pristine graphene-based transparent conductors cannot surpass 90% transmittance and 10 ohm sq^{-1} sheet resistance, which are the ideal metrics for solar cells. Numerous doping methods have been developed to increase the conductivity of graphene, while

Published on 05 October 2016. Downloaded by Xiamen University on 23/11/2017 07:01:38.

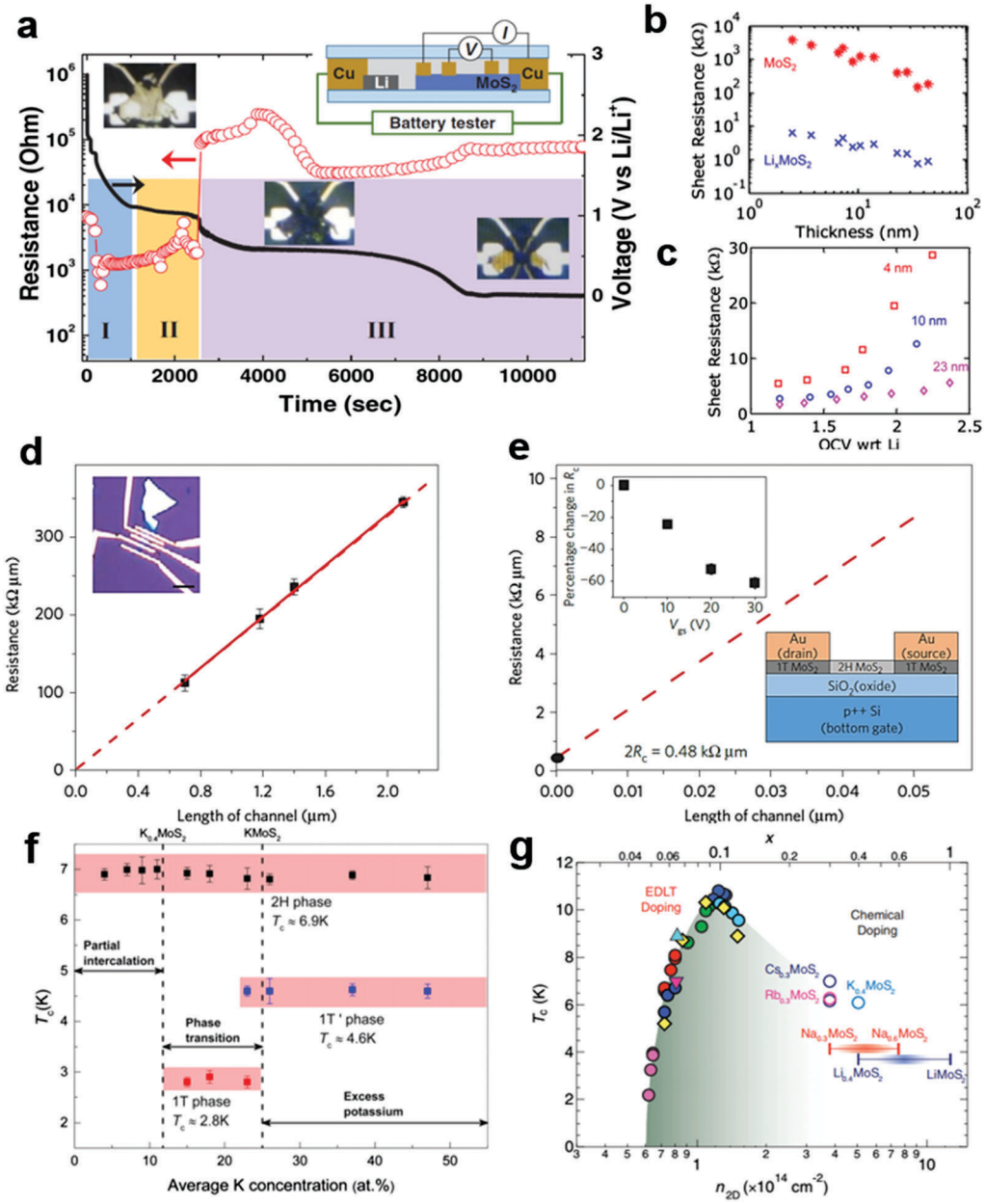

Fig. 6 Electrical properties of tunable metal intercalation in MoS_2 (a) four-probe resistance *vs.* time of MoS_2 sheets undergoing electrochemical lithiation at constant current. Insets show a schematic of the nanobattery setup for *in situ* resistance measurements (upper right), as well as optical images of the lithiated MoS_2 at stages I, II, and III, from left to right.[55] Reproduced with permission from ref. 55. Copyright 2015, John Wiley and Sons. (b) Sheet resistance *vs.* thickness of MoS_2 flakes. A consistent decrease in sheet resistance by more than two orders of magnitude occurs for Li-intercalated MoS_2 as thickness increases. (c) Sheet resistance of Li_xMoS_2 (with thicknesses of 4, 10, and 23 nm) are plotted as a function of their potentials *vs.* Li/Li^+.[124] Reproduced with permission from ref. 124. Copyright 2014, American Chemical Society. (d and e) Resistance *vs.* length of channel plots for MoS_2 FETs. Extrapolation of the red lines yields contact resistances (R_c) of 0.2 kΩ μm for 1T phase contacts at zero gate bias. Inset in (e) shows the percentage decrease in contact resistance with different gate voltages. An optical microscope image and device schematic are also shown as insets in (d and e).[51] Reproduced with permission from ref. 51. Copyright 2015, Nature Publishing Group. (f) Superconducting phases of K intercalated 2H, 1T and 1T′ structured MoS_2.[125] Reproduced with permission from ref. 125. Copyright 2014, American Chemical Society. (g) "Dome-like" superconducting phase diagram of MoS_2 induced by ionic electrolyte gating or metal intercalation.[115] Reproduced with permission from ref. 115. Copyright 2012, American Association for the Advancement of Science.

its transmittance remains unchanged or decreases.[25,93] Recently, a simultaneous increase in both transmittance and conductivity has been demonstrated in few-layer graphene with electrochemical Li intercalation (Fig. 8a).[37] The Li-intercalated few-layer graphene obtained the highest combined metrics for continuous thin film transparent conductors: 91.7% transmittance and 3 ohm sq^{-1} sheet resistance. As shown in the schematic bandstructures of graphene and Li-intercalated graphene (Fig. 8b), this simultaneous increase is achieved by an ultrahigh n-doping from intercalated Li, which fills up the conduction band (high conductivity) and Pauli-blocks the incoming photons even within the visible range (high transmittance). The

 This journal is © The Royal Society of Chemistry 2016

Published on 05 October 2016. Downloaded by Xiamen University on 23/11/2017 07:01:38.

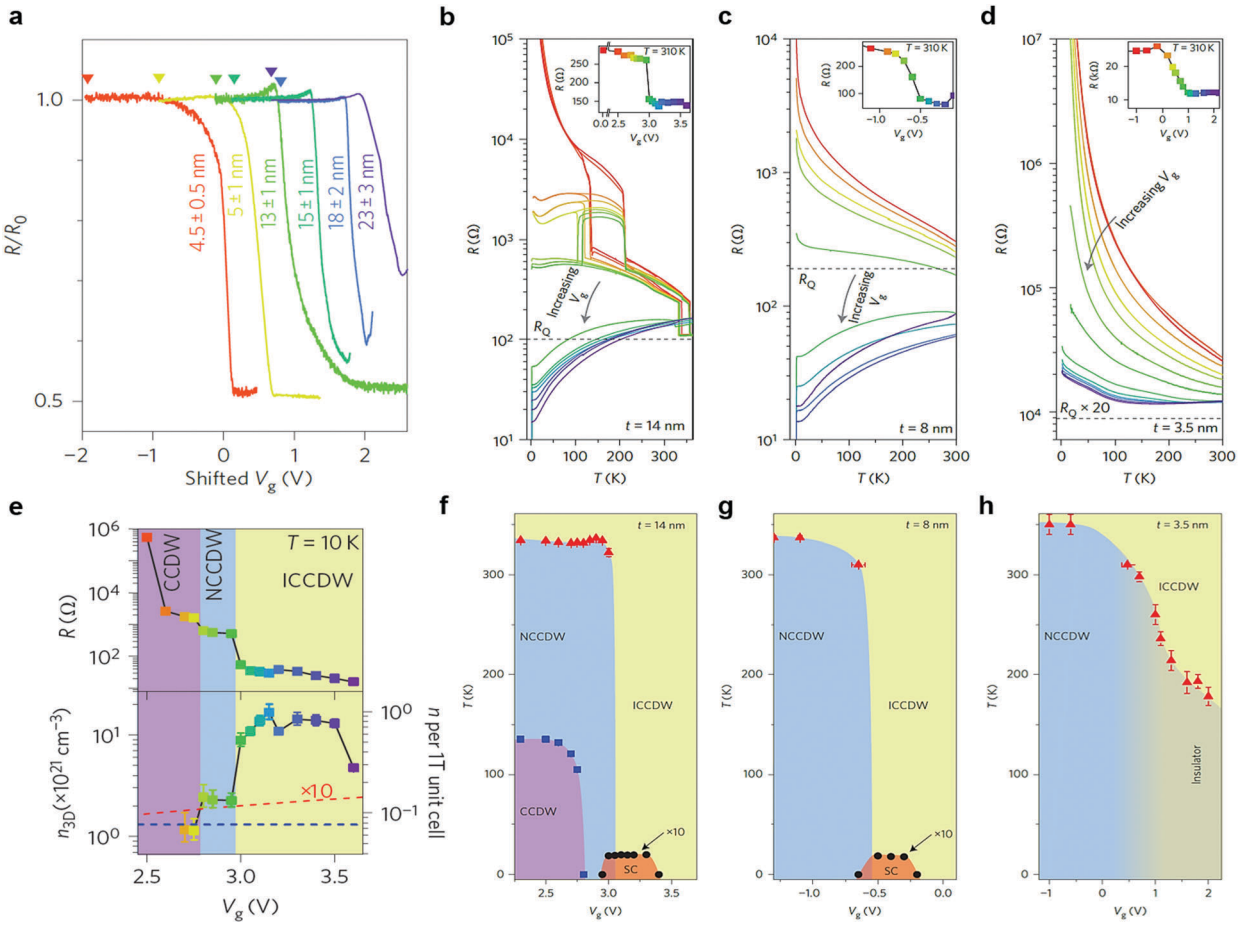

Fig. 7 Electrical properties of Li-intercalated TaS_2 (a) resistance R (normalized to its initial value R_0) shown as a function of V_g for samples with varying thicknesses. The phase transition is manifested as the sudden drop in resistance by one-half. (b–d) Temperature-dependent resistances at fixed V_g for three sample thicknesses: 14 nm, 8 nm and 3.5 nm. The inset in each panel displays the gate-induced phase transition at 310 K. (e) Resistance and volumetric carrier density measured as a function of V_g at 10 K in the same 14 nm-thick sample shown in (b). (f–h) Doping-temperature phase diagrams of 1T-TaS_2 sheets in bulk, quasi-two-dimensional and two-dimensional regimes, respectively.[33] Reproduced with permission from ref. 33. Copyright 2015, Nature Publishing Group.

electrochemical method can precisely control the intercalation process, which also enabled *in situ* and real time characterization of the intercalated graphene (Fig. 8c). A striking difference between intercalated few-layer graphene and bulk graphite is the wavelength-dependent transmittance. As shown in Fig. 8d, intercalated few-layer graphene shows a flat wavelength dependence, while bulk graphite's behavior deviates. A broadband transmittance window from the visible range to the mid-infrared is also believed to open in the intercalated film (Fig. 8e). This technique can also be applied to large-scale, printed reduced graphene oxide networks with earth-abundant Na-ions[128] (Fig. 8f–h).

An alternative approach to improve the performance of graphene-based transparent conductors has been demonstrated with p-type $FeCl_3$ intercalation. Although this type of doping does not increase transmittance in the visible range (induced by Pauli-blocking photons), both the conductivity and overall performance does increase. Additionally, the stability of $FeCl_3$-intercalated few-layer graphene (stability for one year) exceeds many other intercalation compounds.[93] Fig. 9a shows the Raman mapping of G_1 and G_2 peaks before and after high temperature (100 °C) treatment for $FeCl_3$-intercalated few-layer graphene. After 1 hour, the characteristic G_1 and G_2 peaks remain uniform. Thermal cycling of the $FeCl_3$ intercalation compound was also carried out at different temperatures from 50 to 130 °C. However, the sheet resistance of the intercalated flake remains constant, as shown in Fig. 9b. These results indicate the exceptional stability of $FeCl_3$-intercalated few-layer graphene.[129] $FeCl_3$ intercalation was also demonstrated with CVD few-layer graphene that was transferred onto a flexible substrate (Fig. 9c and d).[130] The successful intercalation of $FeCl_3$ in large scale CVD graphene demonstrates the potential commercialization of i2DMs. Note that the work function of the intercalated transparent conductor can be tuned with donor- or acceptor-type intercalants. An all graphene photodetector[131] has also been proposed using $FeCl_3$-intercalated few-layer graphene and pristine graphene heterostructures.

Tuning and understanding the optical properties of semiconducting thin MoS_2 flakes has recently aroused research interests.[55] Like graphite, MoS_2 is well-known as both an electronic and a Li-ion battery electrode material. Thus, it is natural to use the electrochemical method to tune the optical properties of MoS_2 thin flakes upon lithiation. Fig. 10a shows

Published on 05 October 2016. Downloaded by Xiamen University on 23/11/2017 07:01:38.

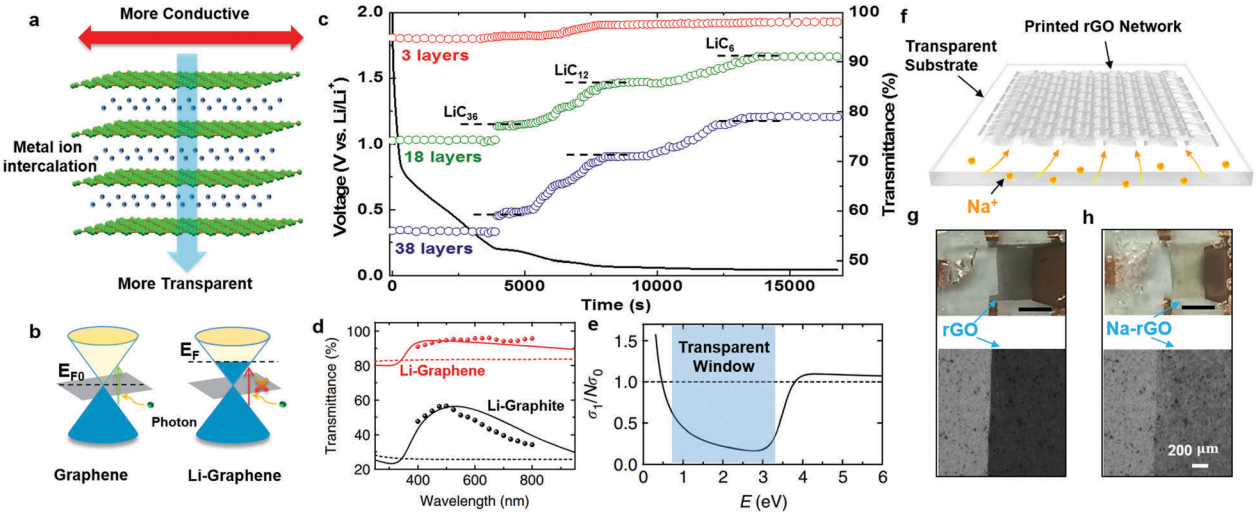

Fig. 8 Optical properties of Li-intercalated few-layer graphene/RGO (a) schematic of metal ion intercalated few-layer graphene. (b) Band structure of graphene before and after Li intercalation. (c) *In situ* transmittance measurements of few-layer graphene upon electrochemical Li intercalation. (d) Experimental and theoretical results of Li-intercalated few-layer graphene and Li-intercalated bulk graphite. (e) Real part of the optical conductivity for Li-intercalated graphene in the broadband.[37] Reproduced with permission from ref. 37. Copyright 2014, Nature Publishing Group. (f) Schematic of printed rGO films on transparent substrates for Na intercalation. Digital and microscope images of printed rGO films (g) before and (h) after Na intercalation.[128] Reproduced with permission from ref. 128. Copyright 2015, American Chemical Society.

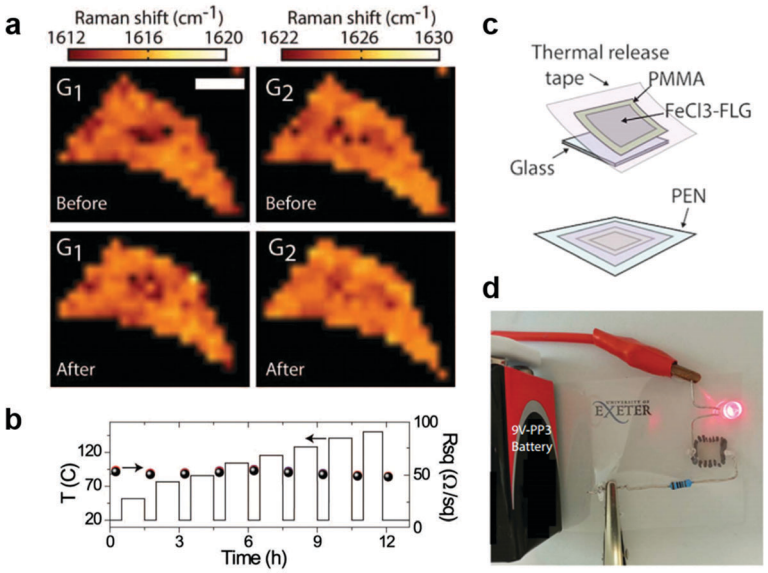

Fig. 9 $FeCl_3$-intercalated few-layer graphene for transparent conductors (a) Raman mapping of the G_1 and G_2 peaks before and after a 1 h 100 °C treatment. (b) R_{sq} changes for $FeCl_3$-intercalated graphene when cycled at different temperatures.[129] Reproduced with permission from ref. 129. Copyright 2015, Nature Publishing Group. (c) Schematic of the dry transfer process for $FeCl_3$-intercalated graphene. (d) Digital image of an $FeCl_3$-intercalated graphene transparent conductor used to light a red LED.[130] Reproduced with permission from ref. 130. Copyright 2015, Nature Publishing Group.

the real time transmittance changes of MoS_2 flakes during lithiation. In this process, the transmittance *vs.* wavelength for the three stages is shown in Fig. 10b: (I) 2H Li–MoS_2, (II) 1T Li–MoS_2 and (III) Li_2S + Mo. A schematic demonstrating the structural changes of converting semiconducting 2H-MoS_2 to metallic 1T Li–MoS_2 is described in Fig. 10c.[50,124] The band structure schematic reveals the origin of substantial changes in the wavelength dependent transmittance between stage I and stage II MoS_2 intercalation compounds (Fig. 10d and e). Digital images of stage I, II, and III intercalated MoS_2 at a wavelength of 450 nm provide a visual representation of the transmittance changes (Fig. 10f–h). The refractive index of stage I and stage II Li–MoS_2 has been obtained by Xiong *et al.*[124] This result is consistent with recent reflectance measurements of 2H-MoS_2 and 1T/1T′ MoS_2 by Brus *et al.*[132] The decrease in the imaginary part of the refractive index also supports the reduced absorption of 1T-LiMoS_2 (Fig. 10i and j). Another important application of Li intercalation in MX_2 materials is exfoliating into monolayer MX_2

 This journal is © The Royal Society of Chemistry 2016

Published on 05 October 2016. Downloaded by Xiamen University on 23/11/2017 07:01:38.

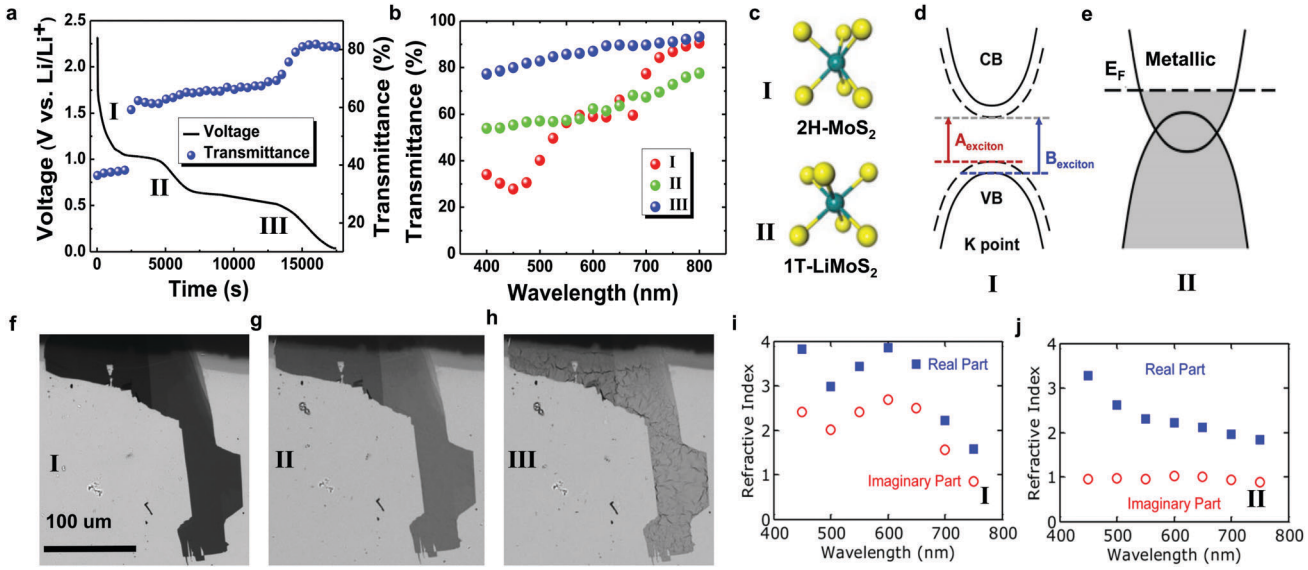

Fig. 10 Optical properties of tunable Li intercalation in MoS_2. (a) *In situ* transmittance measurements of few-layer MoS_2 upon electrochemical Li intercalation. (b) Transmittance in the visible range of ion intercalated MoS_2 at different stages.[55] Reproduced with permission from ref. 55. Copyright 2015, John Wiley and Sons. (c) Schematic of MoS_2 2H and 1T phases. Band structure schematics for (d) MoS_2 and (e) $LiMoS_2$.[50] Reproduced with permission from ref. 50. Copyright 2013, National Academy of Sciences, USA. (f–h) Microscope images of MoS_2 crystallites upon Li intercalation at three different stages at a wavelength of 450 nm. Refractive index *vs.* wavelength for (i) MoS_2 and (j) $LiMoS_2$.[124] Reproduced with permission from ref. 124. Copyright 2015, American Chemical Society.

flakes. Monolayer MoS_2 flakes with a direct band gap, large lateral dimensions and excellent photoluminescence properties have been successfully prepared by intercalated liquid exfoliation methods.[133] Note that the previously described studies provide examples of tuning the optical properties of MX_2 only through Li intercalation. Due to the large van der Waals gap between MX_2 layers, more intercalation species can be accommodated in the interlayer spacing. Therefore, further investigation of these MX_2 materials should be pursued to ascertain their optical properties.

Electrochemical intercalation allows the modulation of photoluminescence (PL) in MoS_2 flakes. Fig. 11a–g exhibits

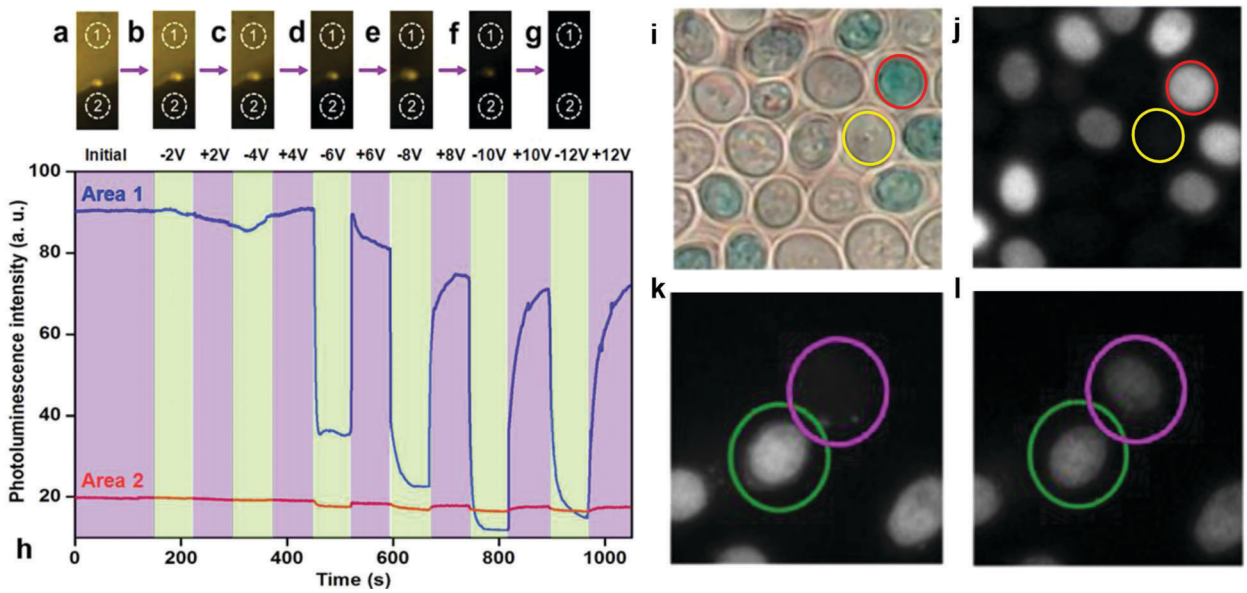

Fig. 11 Intercalation tuned MoS_2 photoluminescence (a–g) PL images of MoS_2 films at different intercalation voltages. (h) *In situ* PL intensities of MoS_2 flakes due to the electrochemical intercalation/deintercalation process.[134] Reproduced with permission from ref. 134. Copyright 2013, American Chemical Society. (i) Digital and (j) PL images of the MoS_2–yeast cell system. The cells circled in red and yellow are nonviable and viable cells, respectively. Fluorescent images of yeast cells (viable = purple circle; nonviable = green circle) after adding methanol for (k) 0 s and (l) 6000 s.[135] Reproduced with permission from ref. 135. Copyright 2014, American Chemical Society.

Published on 05 October 2016. Downloaded by Xiamen University on 23/11/2017 07:01:38.

the PL images of MoS_2 flakes modulated by electrochemical intercalation of Li-ions, Na-ions and K-ions. The intercalation induced electronic structure changes and/or phase changes drive the PL response. The modulation process is reversible and the effect becomes more obvious as the intercalation bias increases[134] (Fig. 11h). Additionally, this effect was utilized to observe the enzymatic activities and cell viabilities of biological systems.[135] Fig. 11i and j shows the optical and fluorescent images of yeast cells coated with MoS_2 nanoflakes. Note that the red and yellow circles correspond to the nonviable and viable cells, respectively. Unlike the viable cells, the nonviable cells produce strong PL signals. When the cells are immersed in a low K^+ buffer solution, the ion concentration differences within and outside the cells drives K^+ movement and enables K^+ to intercalate within the coated MoS_2 flakes. After 6000 s of immersion, the viable cells obtain PL signals comparable to the nonviable ones, which demonstrates the ability to investigate cell viability by intercalation methods (Fig. 11k and l).

Besides the electrochemical intercalation of metal ions, other intercalation methods and guest species have been employed. Among them, zerovalent metal intercalation of Bi_2E_3 (E = S, Se) materials and metal oxides have attracted tremendous attention (Fig. 12a–c).[136–138] Zerovalent metal intercalation of Bi_2E_3 causes alterations in its electronic band structure (Fig. 12d) and induces optical property changes in both the visible (Fig. 12e) and the near-infrared range (Fig. 12f). Co-intercalation of various zerovalent metals in these layered materials have also been demonstrated.[139] Chemically intercalated Bi_2E_3 using organic intercalation species can induce plasma peak shifts in the host material (Fig. 12g–i).[137] A recent study on the chemical intercalation of zerovalent metals in metal oxides revealed a reversible intercalation process with potential for chemochromic applications (Fig. 12j–l).[140] Overall, intercalation has been demonstrated as a very effective way to change the optical properties of 2D materials. We believe that rational i2DM designs could lead to further 2D material advances for photonic and optoelectronic devices.

6. Tuning thermal and thermoelectric properties

Beyond the synergistic enhancement of conductivity and optical transmittance for transparent conductors, intercalation can lead to similar advances in thermoelectrics. In addition to electrical conductivity modulation, the introduction of guest species in the 2D material's van der Waals gap alters its thermal properties since phonon propagation can be effectively tuned by intercalation-induced structural changes. For a given thermoelectric material, the ability of generating thermoelectric power is determined by its dimensionless figure of merit: $ZT = \sigma S^2 T/\rho$ where S, σ, ρ, and T are the Seebeck coefficient, electrical conductivity, thermal conductivity and absolute temperature, respectively. One approach to increase ZT is to suppress thermal conductivity while maintaining or even increasing the material's electrical conductivity. In this manner, the intercalation method can provide a new avenue to tune 2D materials for thermoelectric applications. Despite the extraordinary thermal properties of 2D materials compared with their bulk counterparts,[141,142] the thermal properties of i2DMs are rarely investigated. In this section, we will discuss the recent progress of layered materials with improved thermal or thermoelectric properties by intercalation methods. Note that we anticipate more research focusing on the thermal properties of i2DMs in the near future.

Wan *et al.* reported that intercalating a SnS layer into layered TiS_2 (Fig. 13a) can improve the thermoelectric performance in the parallel and perpendicular directions with respect to the

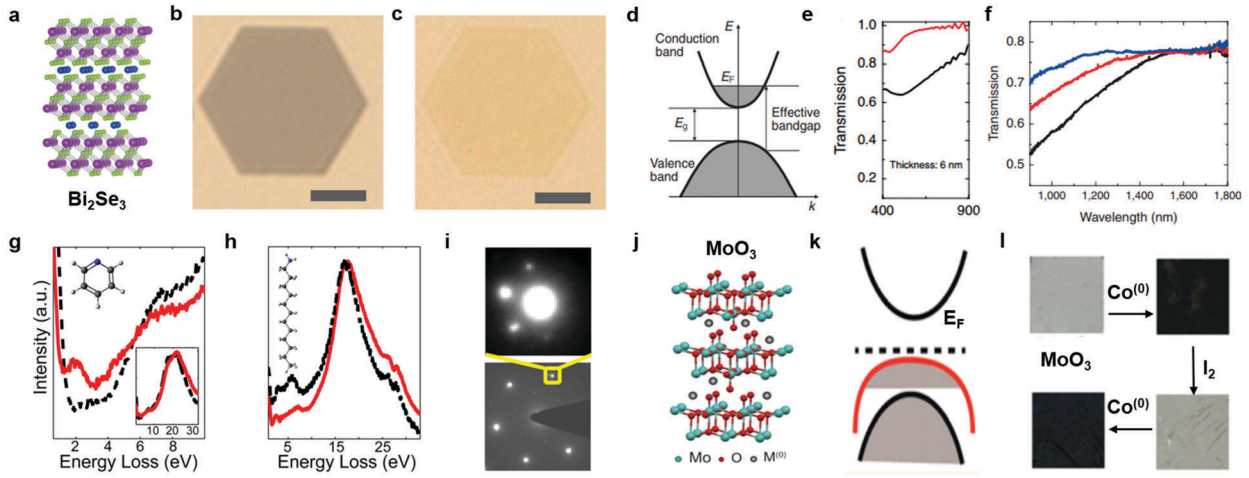

Fig. 12 Optical and photonic properties of zerovalent metal and organic i2DMs. (a) Schematic of Cu-intercalated Bi_2Se_3. Microscope image of Bi_2Se_3 (b) before and (c) after Cu intercalation. (d) Band structure of Cu-intercalated Bi_2Se_3. Optical transmittance of Bi_2Se_3 over the (e) visible and (f) near-infrared spectral range before and after Cu intercalation.[136] Reproduced with permission from ref. 136. Copyright 2014, Nature Publishing Group. (g–i) EELS and diffraction patterns of Bi_2Se_3 intercalated with organic molecules.[137] Reproduced with permission from ref. 137. Copyright 2013, American Chemical Society. Schematics of zerovalent metal intercalated MoO_3: its (j) crystal structure and (k) band structure. (l) Digital images of the reversible intercalation of Co metal in MoO_3.[140] Reproduced with permission from ref. 140. Copyright 2015, American Chemical Society.

 This journal is © The Royal Society of Chemistry 2016

Published on 05 October 2016. Downloaded by Xiamen University on 23/11/2017 07:01:38.

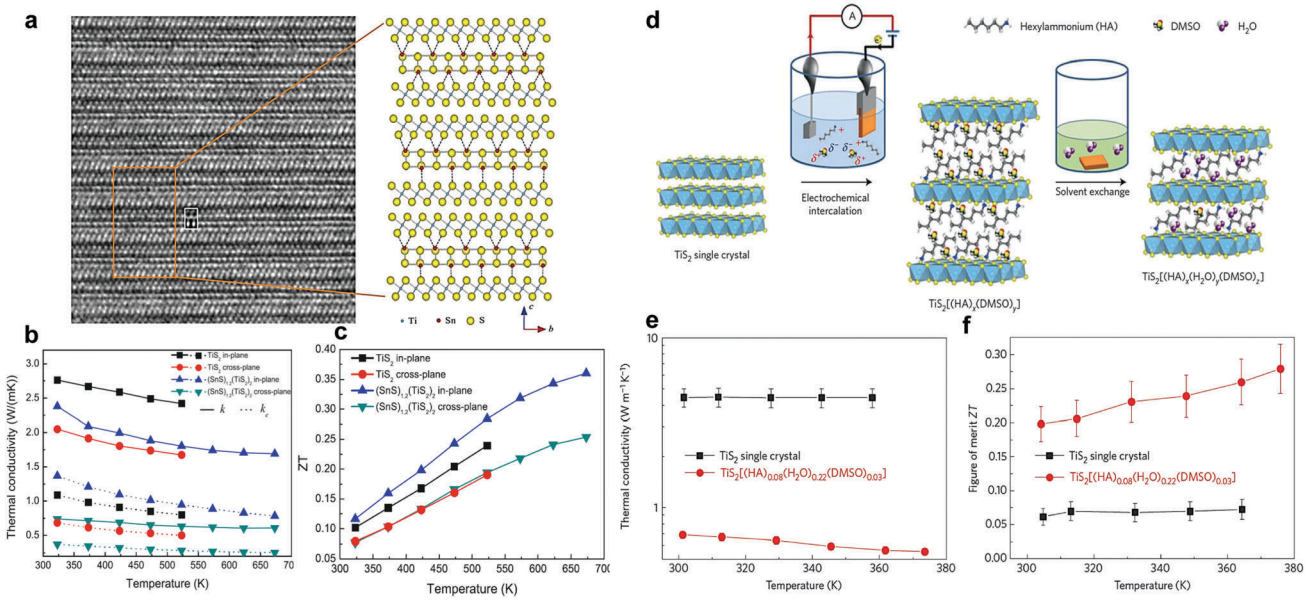

Fig. 13 Tunable thermoelectric properties for intercalated TiS_2 (a) high resolution TEM image of $(SnS)_{1.2}(TiS_2)_2$ along the [100] zone axis. The zoom-in image depicts the actual crystal structure of $(SnS)_{1.2}(TiS_2)_2$ reconstructed from the area indicated in the HRTEM image. (b) Total thermal conductivities k and the electron component k_e of TiS_2 and $(SnS)_{1.2}(TiS_2)_2$ in both the in-plane and cross-plane directions. (c) ZT values of TiS_2 and $(SnS)_{1.2}(TiS_2)_2$ in both the in-plane and cross-plane directions.[143] Reproduced with permission from ref. 143. Copyright 2015, Springer. (d) The process to electrochemically intercalate a TiS_2 single crystal to create a $TiS_2[(HA)_x(H_2O)_y(DMSO)_z]$ superlattice. (e) In-plane thermal conductivity *vs.* temperature. (f) In-plane thermoelectric figure of merit *vs.* temperature.[54] Reproduced with permission from ref. 54. Copyright 2015, Nature Publishing Group.

layers.[143] This decrease in thermal conductivity occurs through softening of the transverse sound velocities as well as vertically localizing phonons (Fig. 13b). Therefore, the ZT value of $(SnS)_{1.2}(TiS_2)_2$ is significantly enhanced in the in-plane direction (Fig. 13c) and remains nearly constant in the cross-plane direction due to simultaneous scattering of both electrons and phonons. The same group also used organic cations ($(hexylammonium)_x$-$(H_2O)_y(DMSO)_z$) as an intercalant to create a flexible hybrid superlattice (Fig. 13d).[54] Through intercalation, the thermoelectric properties and the figure of merit, ZT, is dramatically improved: 0.28 *vs.* <0.08 at 373 K (Fig. 13e and f).

The electrochemical intercalation of Li effectively modulates the thermal conductivity of lithium cobalt oxide ($LiCoO_2$), a layered crystal commonly used as a Li-ion battery cathode. Cho *et al.* designed an *in situ* measurement cell (Fig. 14a) to probe the thermal conductivity during lithiation.[144] The representative time-domain thermoreflectance (TDTR) data shown in Fig. 14b was used to extract the thermal conductivity of lithiated and delithiated Li_xCoO_2 films. The work demonstrated that both the thermal conductivity and the elastic modulus adjusts significantly as $Li_{1.0}CoO_2$ changes to $Li_{0.6}CoO_2$ (Fig. 14c and d). The composition dependence suggests that the change in thermal conductivity with decreasing Li concentration is related to not only the softening of the lattice but also to the Li_xCoO_2 phase behavior.

The manipulation of thermal properties by intercalation could be applied to numerous 2D materials and a range of intercalants including atoms, ions and molecules with various sizes and charges. The method can also be applied when the host material is further diversified with the 2D hybrid structures. In this manner, intercalation provides a new avenue to optimize thermoelectric performance and the study of i2DMs could offer even more rewarding outcomes.

7. Tuning magnetic properties

Intercalating magnetic species into the host 2D materials widely tunes its magnetic properties. The magnetic properties of i2DMs should be different from its bulk counterparts due to reduced interplanar magnetic coupling. Bointon *et al.* demonstrated the successful intercalation of large area multilayer epitaxial graphene with $FeCl_3$ (Fig. 15a).[52] Fig. 15b shows the measured weak localization signal at different temperatures, where the phase coherence length L_ϕ can be extracted (Fig. 15c). Between 280 mK and 80 K, the estimated L_ϕ of $FeCl_3$/few-layer graphene is much larger than previously reported pristine graphene: $L_\phi \approx 1.2$ μm at 280 mK. The observed temperature dependence of L_ϕ is also compatible with the occurrence of magnetic ordering in stage one $FeCl_3$/few-layer graphene. Morosan *et al.* reported that Fe can be intercalated into layered TaS_2 to modify its magnetic properties (Fig. 15d).[53,145] Fig. 15e and f displays the magnetoresistance (MR) measurements of bulk and exfoliated thin sheets of $Fe_{0.28}TaS_2$ at different temperatures. In both cases, the largest $\Delta\rho/\rho_0$ (close to 60%) was observed at $T = 4$ K. However, the transitions at H_S are much sharper in the bulk material than in the 2D form at lower temperatures. This may imply that long range interlayer coupling between the Fe ions in different layers is weakened in the 2D crystals. The temperature dependence on switching field H_S and MR peak

Published on 05 October 2016. Downloaded by Xiamen University on 23/11/2017 07:01:38.

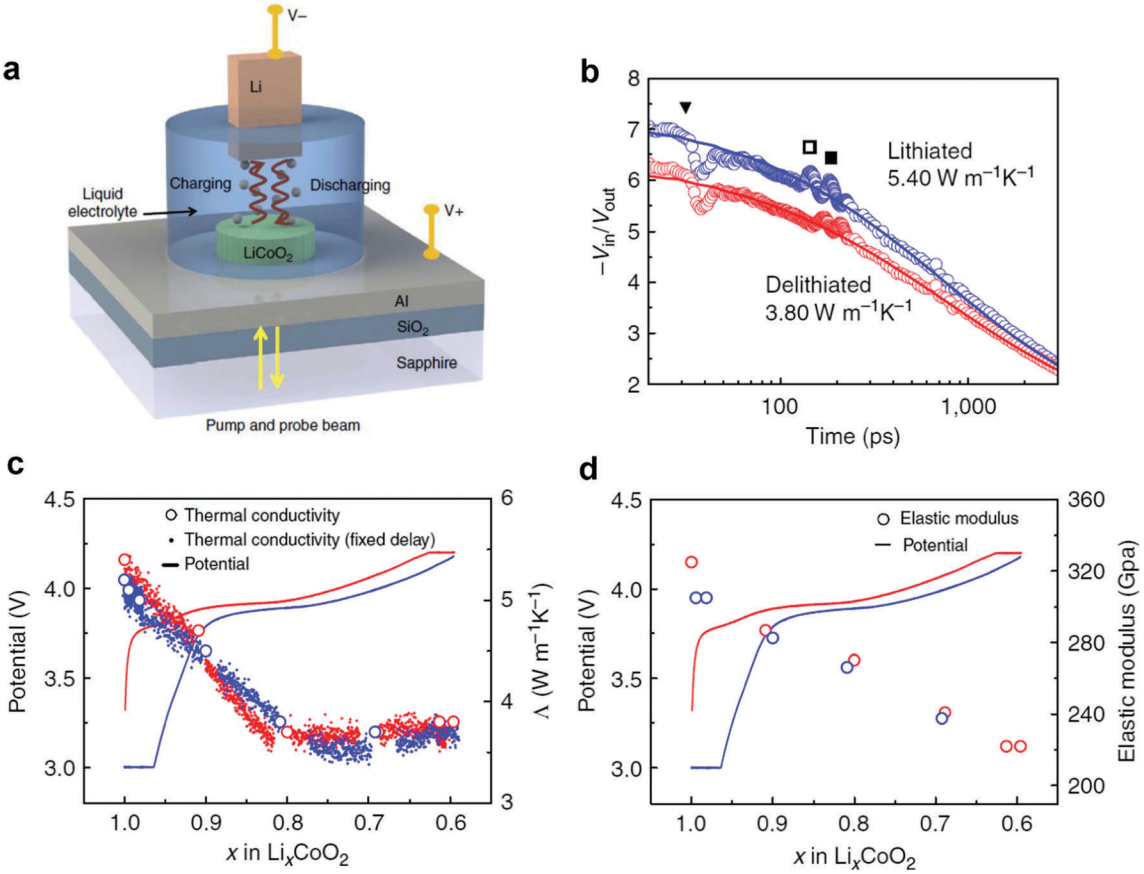

Fig. 14 Thermal properties of tunable Li intercalation in $LiCoO_2$. (a) Schematic of the *in situ* measurement cell consisting of ~500 nm $LiCoO_2$, a 70 nm Al transducer and a 100 nm SiO_2 thermal isolation layer on a sapphire substrate. (b) TDTR data (open circles) and thermal conductivity fit (lines) for representative lithiated (x = 1.0) and delithiated (x = 0.6) Li_xCoO_2. (c) Thermal conductivity and potential as a function of Li insertion. (d) The lithiation-dependent longitudinal elastic modulus of Li_xCoO_2 calculated from the longitudinal speed of sound. In both (c) and (d), the data in red and blue corresponds to the delithiation and lithiation process, respectively.[144] Reproduced with permission from ref. 144. Copyright 2014, Nature Publishing Group.

height for both bulk and 2D crystals is also similar (Fig. 15e). However, the MR peak height increased monotonically with decreasing temperature for the 2D crystals while the bulk crystal increased until a maximum at 4 K and then decreased at lower temperatures (Fig. 15f).

8. Tuning energy storage properties

Electrochemical capacitors and ion batteries have attracted tremendous interest for the past few decades due to an increasing need for clean and sustainable energy storage systems.[20,146–148] For practical devices, researchers search for materials that provide both high energy density and high power density. Typically, electrochemical capacitors, also known as supercapacitors, store energy in an electrical double layer where charged ions build up on the electrode surface. This enables a rapid charge/discharge process but stores a limited amount of energy. On the contrary, ion batteries store ions *via* electrochemical reactions where ions typically diffuse between the electrodes upon charging/discharging. Diffusion is typically a slow process but the energy stored exceeds supercapacitors. Therefore, improving the energy density of capacitors and power density of ion batteries is of great interest. Through intercalation methods and tunable electrode materials, the performance of energy storage systems can be improved.

MoS_2 is not a typical supercapacitor material due to its stable 2H semiconducting phase, however, Acerce *et al.* demonstrated that metallic 1T-MoS_2 can act as a high-performance supercapacitor electrode material through intercalation methods.[149] Note that these flakes can be re-stacked together to form flexible electrodes (Fig. 16a and b). The 1T-MoS_2 electrode can be rapidly intercalated with protons, Li-ions, Na-ions, or K-ions with capacitances ranging from 400 to 700 F cm^{-3} in aqueous electrolytes (Fig. 16c). Chhowalla and coworkers identified increases in the interlayer distance depending on the type of solvated ions intercalated into MoS_2 (Fig. 16d). The electrode can also operate under high voltages in nonaqueous solutions.

Using a special intercalation method, tunably intercalated MoS_2 has been shown to act as both a high power and energy density electrode through *in situ* observations.[55] As mentioned in the previous section, the planar micro-battery our group developed enabled the electrochemical intercalation of 2D

 This journal is © The Royal Society of Chemistry 2016

Published on 05 October 2016. Downloaded by Xiamen University on 23/11/2017 07:01:38.

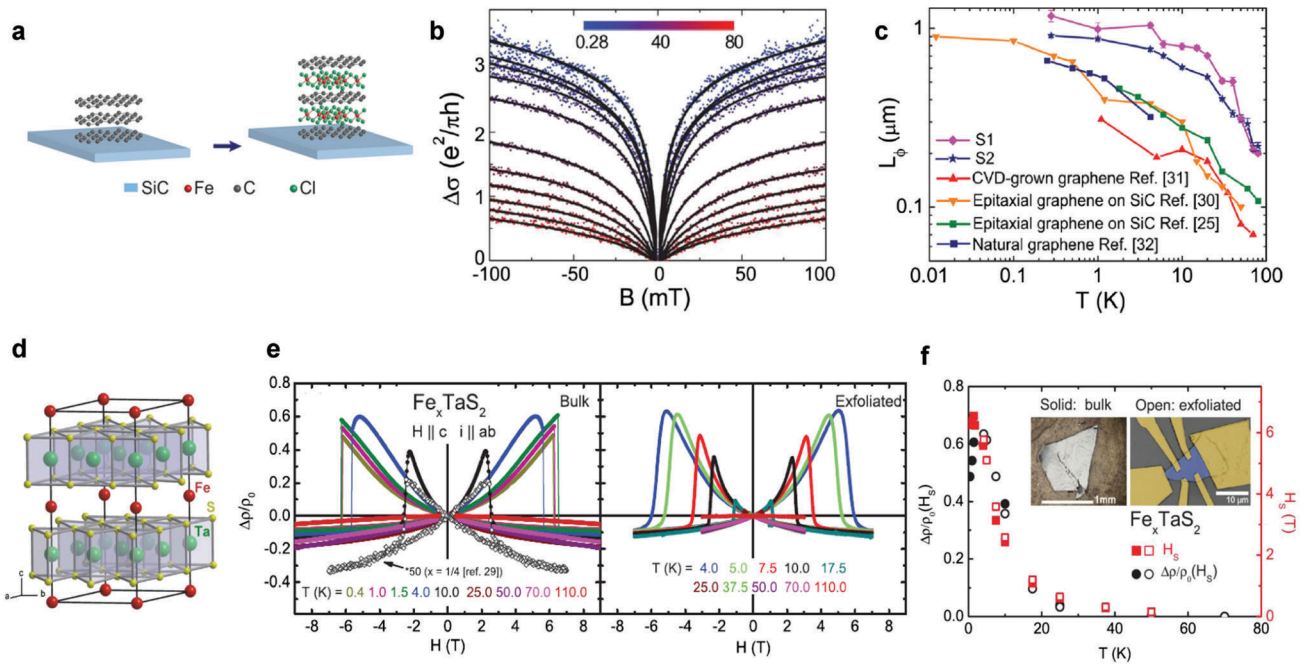

Fig. 15 Magnetic properties of metal/molecule i2DMs. (a) Schematic crystal structure of trilayer $FeCl_3$/graphene. (b) The measured weak localization contribution to the magneto-conductance (scatter points) and theoretical fits (solid line). (c) The temperature dependence of L_ϕ for pristine graphene prepared by different methods. The values are compared to the estimated values of $FeCl_3$/few-layer graphene.[52] Reproduced with permission from ref. 52. Copyright 2014, American Chemical Society. (d) The crystal structure of $Fe_{0.25}TaS_2$.[53] Reproduced with permission from ref. 53. Copyright 2007, American Physical Society. (e) Measurement of magnetoresistance $\Delta\rho/\rho_0$ for bulk and thin $Fe_{0.28}TaS_2$ devices at selected temperatures for $H\|c$ axis, and $i\|ab$-plane. (f) Comparison of H_S and $\Delta\rho/\rho_0$ peak height values as a function of temperature for bulk (solid symbols) and thin 2D devices. The inset displays a typical bulk sample (left) and an exfoliated sample with metal contacts (right).[145] Reproduced with permission from ref. 145. Copyright 2015, American Physical Society.

materials as well as *in situ* monitoring of the resistance changes of MoS_2 flakes upon intercalation (Fig. 16e). Note that Mo and Li_2S are formed at the final lithiation stage when MoS_2 is used as a Li-ion battery electrode. The insulating Li_2S hinders electron transport in this material, which prevents MoS_2 to act as a high power and energy dense electrode. However, using a special "rapid" lithiation process, the resistance of the lithiated MoS_2 flake at the final stage reduced by 1000 times. This resistance decrease, which was measured using the *in situ* planar battery set-up, led to a three-fold increase in specific capacity and the cell showed stable cycling performance compared to the conventional lithiated MoS_2 (Fig. 16f). The results illustrate the importance of *in situ* techniques to monitor and understand the resistance changes of battery electrodes in real time.[55] Additionally, the "rapid" intercalation process can be adopted for other 2D materials to modify and enhance electrochemical performance.

9. Tuning catalytic properties

Tremendous research attention has been given to electrocatalysis for effective, low cost hydrogen generation. The typical hydrogen evolution process *via* electrocatalysis undergoes a three step mechanism. First, protons are adsorbed on the electroactive sites, while electrons that are transferred to the adsorbed protons form the adsorbed H atoms. H_2 gas begins to form from the adsorbed H atoms and desorbs due to the presence of an electrocatalyst. It is well known that platinum (Pt) group metals offer the best electrocatalytic performance, however, the cost of these noble metals is exorbitant. Therefore, finding a cost-efficient replacement for an electroactive, electrochemically stable catalyst has challenged researchers for decades. Recently, 2D TMDs such as MX_2 (M = Mo, W; X = S, Se) have emerged as promising HER electrocatalysts.[12,150,151] The general design principles for high-performance 2D TMD electrocatalysts include: (1) increasing the number and activity of catalytic sites as well as (2) increasing the charge transport during the catalytic process. Various nanostructures have been reported to increase the active edge sites of 2D TMDs as well as the conductivity between the catalytic material and the conductive substrate, which leads to high-performance composite electrocatalytic materials. However, for 2D TMD nanosheets, the low density of metallic catalytically active sites and their overall semiconducting nature hinders the material's overall catalytic performance. Therefore, intrinsically improving the catalytic activity and electronic conductivity of 2D TMD materials will lead to major enhancements in catalytic performance.

Intercalation provides a unique approach to optimize the catalytic activities of MX_2 materials. We previously mentioned that Li intercalation in MX_2 materials (such as MoS_2) not only facilitates the exfoliation of bulk materials, but also induces

Published on 05 October 2016. Downloaded by Xiamen University on 23/11/2017 07:01:38.

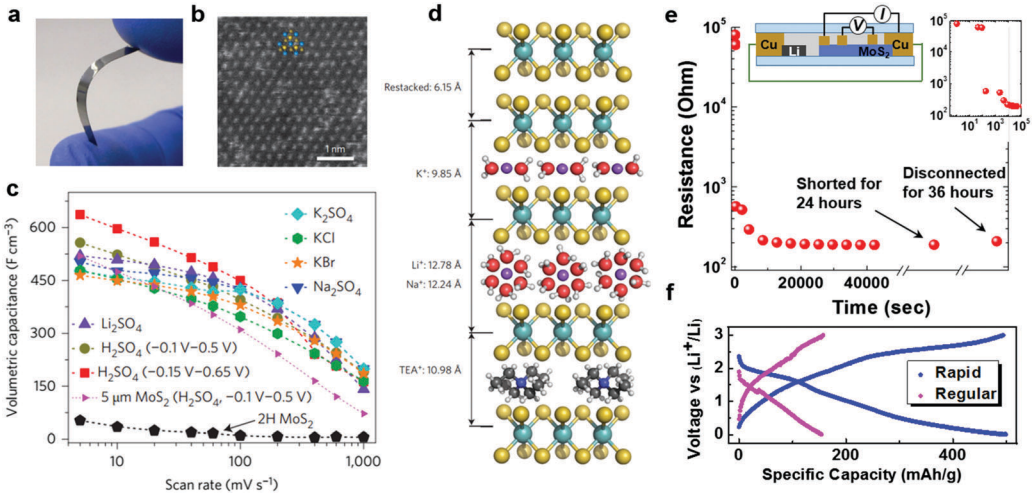

Fig. 16 Enhanced energy storage properties for tunable Li-intercalated MoS_2 (a) digital image of a flexible 1T-MoS_2 electrode. (b) HRTEM image of 1T-MoS_2. (c) Capacitance of 1T-MoS_2 electrodes in various solutions. (d) Schematic of MoS_2 intercalated with different solvated ions.[149] Reproduced with permission from ref. 149. Copyright 2015, Nature Publishing Group. (e) *In situ* resistance measurements of MoS_2 upon lithiation. (f) Electrochemical performance of rapid and conventionally lithiated MoS_2 as a Li-ion battery anode.[55] Reproduced with permission from ref. 55. Copyright 2015, John Wiley and Sons.

phase changes such as a conversion from a semiconducting 2H phase to a metallic 1T phase.[92,150] This intercalation-induced phase change is ideal for electrocatalysis since it enhances both the material's catalytic activity and electronic conductivity. Voiry *et al.* demonstrated significant improvements in the HER activity of 1T WS_2 by chemically intercalating and exfoliating 2H WS_2.[94] From DFT calculations, Chhowalla and coworkers demonstrated that a distorted 1T structure will provide greater catalytic performance due to the lower reaction free energy. Lukowski *et al.* obtained similar results for both chemically intercalated 1T MoS_2 and 1T WS_2 nanoflowers (Fig. 17a–f).[150,152] An outstanding overpotential of −142 mV *vs.* RHE at 10 mA cm^{-2} was achieved with 1T WS_2 nanoflowers, which corroborates the potential of intercalation tuned MX_2 electrocatalysts.

Vertically aligned MoS_2 nanoflakes can also act as high-performance HER catalysts after electrochemical Li intercalation (Fig. 17g).[50,153] Unlike chemical intercalation, electrochemical intercalation is more controllable, which allows the catalytic

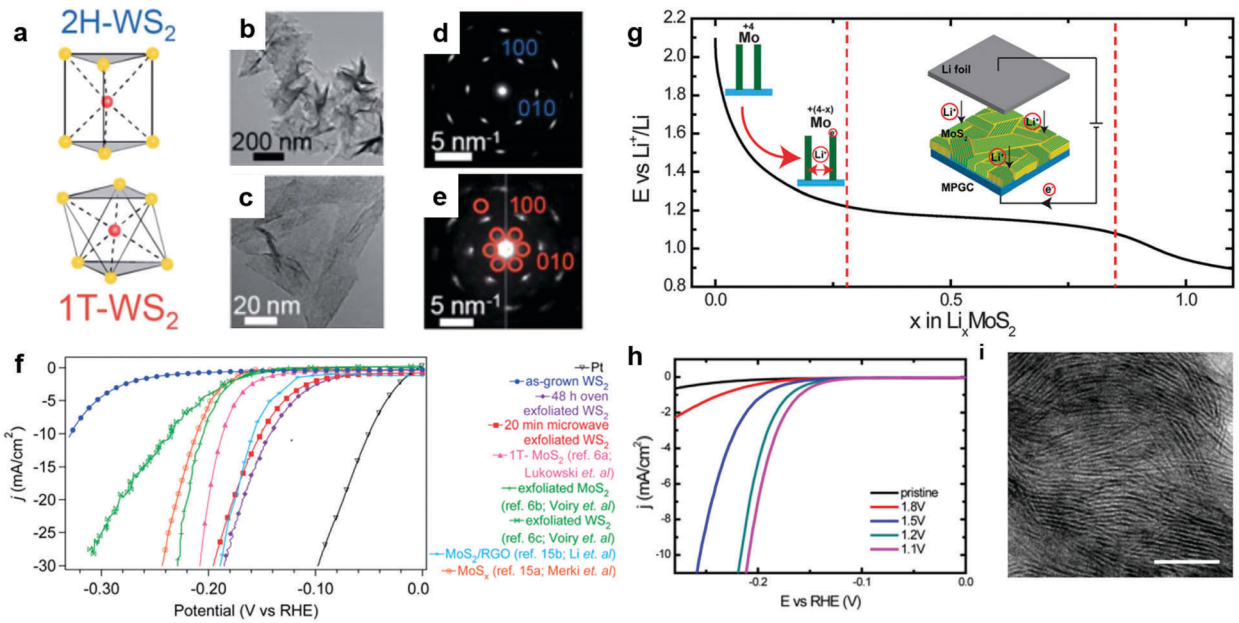

Fig. 17 Tunable catalytic properties for Li-intercalated MX_2 2D materials (a) schematic of WS_2 with 2H and 1T phases. (b and c) TEM images and (d and e) diffraction patterns of WS_2 before and after Li intercalation. (f) Tafel plot of different forms of MoS_2 and WS_2 catalysts. (g) Electrochemical preparation of 1T-MoS_2 for water splitting.[150] Reproduced from ref. 150. Copyright 2014, Royal Society of Chemistry. (h) Tafel plot of electrochemically and tunably intercalated MoS_2 as a water splitting catalyst. (i) SEM image (top view) of the 1T-MoS_2 catalyst.[50] Reproduced with permission from ref. 50. Copyright 2013, National Academy of Sciences, USA.

 This journal is © The Royal Society of Chemistry 2016

Published on 05 October 2016. Downloaded by Xiamen University on 23/11/2017 07:01:38.

Table 3 Summary of intercalation in 2D layered materials, properties and applications

Material types	Graphene family	Metal dichalcogenides (MX_2)	Other chalcogenides (MX, M_2X_3)	Layered oxides
2D materials (properties)	Graphene, rGO, BN (semimetal)	MoS_2, WS_2, TiS_2 (semiconductors) TaS_2, $NbSe_2$ (metals) $TiSe_2$ (semimetal)	Bi_2Se_3, Sb_2Te_3 (topological insulators) In_2Se_3 (semimetal) GaSe (semiconductor) FeSe (metal)	$LiCoO_2$, MoO_3 (insulators)
Intercalation species/products	Ions (Li^+, Na^+, K^+, Ca^{2+}, PF_6^-, ClO_4^-, *etc.*) Inorganic (Br_2, $FeCl_3$ *etc.*)	Ions (Li^+, Na^+, Mg^{2+}, *etc.*) Organic molecules Zerovalent metals (Cu, Sn, Co, *etc.*) Phase change	Zerovalent metals (Cu, Sn, Co, *etc.*) Organic molecules Co-intercalants	Zerovalent metals (Cu, Sn, Co, *etc.*) Ions (Li^+)
Methods	Chemical and electrochemical intercalation			
Tuning properties/ applications	Electrical, optic, optoelectronic, magnetic	Electrical (superconductor, CDW), optic, catalytic, thermoelectric, magnetic	Electrical (superconductor), optic, optoelectronic	Thermal, catalytic optic, chemochromic

activity of MoS_2 at various Li concentrations to be studied. Surprisingly, Wang *et al.* demonstrated that the catalytic performance improves as the Li concentration increases even before the 2H to 1T phase transition occurs. This behavior transpires through changes in both the material's electronic structure and its doping levels (*i.e.* electron doping of the Mo d-band) due to Li intercalation. The highest catalytic performance of MoS_2 corresponds to 1T MoS_2 that is electrochemically intercalated at 1.1 V (Fig. 17h and i). As more Li is intercalated, the catalytic performance decreases due to the formation of inactive Mo and Li_2S. A variety of nanostructures using intercalation tuned MX_2 electrocatalytic materials has been investigated in a similar manner. Note that the electrochemical intercalation method not only applies to MX_2 HER electrocatalysts but also other layered materials. For instance, electrochemically intercalated layered materials, such as $LiCoO_2$,[154] have a wide range tunability, and can act as electrocatalysts. Unlike the electrochemical intercalation method, this behavior is not possible *via* chemical intercalation methods.

10. Conclusion and outlook

In summary, we provide a comprehensive review of the recent progress on i2DMs. Host materials, various intercalation species and intercalation methods as well as tunable properties and potential applications enabled by intercalation are discussed (Table 3). The numerous intercalation methods widely tune the physical and chemical properties of the host 2D materials, resulting in excellent performing i2DMs over a wide range of applications. Although intensive studies of intercalation in layered bulk materials have been performed, investigations of i2DMs are still in the early stages. The future research of i2DMs relies on additional fundamental studies and the scalable application of i2DMs.

For fundamental studies, a rational design of the host materials and intercalation species is critical for the investigation of i2DMs with novel properties. Selective intercalation in few-layer graphene can result in bandgap opening.[155,156] van der Waals heterostructured 2D materials would provide an excellent platform to study the interfacial storage mechanism as well as other intriguing physical and chemical properties of intercalated van der Waals heterostructures.[157] Co-intercalation of different intercalant species in one host 2D material could lead to unforetold properties of i2DMs compared to single intercalated materials. Intercalation controlled mechanical properties (*e.g.* friction) of i2DMs could yield additional insight into this field. Further improvements on *in situ* platforms could uncover novel properties of i2DMs in real time. The reversible modulation of 2D materials by intercalation in broader wavelengths other than the visible range (*i.e.* terahertz and infrared) is also desired for telecommunication and military uses.

For future applications, issues such as stability, scalability and the manufacturing cost of i2DMs need to be addressed. Many i2DMs are unstable and degrade in air. Therefore, the rational design of i2DMs and their encapsulation is of great importance for scalable and practical applications. Cost-effective, high performance host 2D materials can further the development of i2DMs for use as transparent electrodes, electrochromic devices, 2D flexible energy storage devices and lightweight conductors.[158] Currently, relatively slow ion transport limits the use of i2DMS for high speed electronics. However, i2DMs have potential as low frequency, high power, flexible electronic devices. With further in-depth studies, i2DMs will rapidly develop and have great potential in commercial device applications.

Acknowledgements

L. Hu acknowledges the support from NSF Grants 1335944 and 1335979. This work is also partially supported as part of the Nanostructures for Electrical Energy Storage (NEES), an Energy Frontier Research Center funded by the US Department of Energy, Office of Science, Basic Energy Sciences under Award number DESC0001160. M. S. Fuhrer acknowledges support from an Australian Research Council Laureate Fellowship and Discovery Project. W. Bao acknowledges the support by National Key Research and Development Program under Award number 2016YFA0203900. S. D. Lacey acknowledges the support by the Department of Defense (DoD) through the National Defense Science and Engineering Graduate (NDSEG) Fellowship Program.

Published on 05 October 2016. Downloaded by Xiamen University on 23/11/2017 07:01:38.

References

1 A. K. Geim and K. S. Novoselov, *Nat. Mater.*, 2007, **6**, 183–191.
2 S. Z. Butler, S. M. Hollen, L. Y. Cao, Y. Cui, J. A. Gupta, H. R. Gutierrez, T. F. Heinz, S. S. Hong, J. X. Huang, A. F. Ismach, E. Johnston-Halperin, M. Kuno, V. V. Plashnitsa, R. D. Robinson, R. S. Ruoff, S. Salahuddin, J. Shan, L. Shi, M. G. Spencer, M. Terrones, W. Windl and J. E. Goldberger, *ACS Nano*, 2013, **7**, 2898–2926.
3 M. Chhowalla, H. S. Shin, G. Eda, L.-J. Li, K. P. Loh and H. Zhang, *Nat. Chem.*, 2013, **5**, 263–275.
4 H. Zhang, *ACS Nano*, 2015, **9**, 9451–9469.
5 H. Li, J. M. T. Wu, Z. Y. Yin and H. Zhang, *Acc. Chem. Res.*, 2014, **47**, 1067–1075.
6 Q. H. Wang, K. Kalantar-Zadeh, A. Kis, J. N. Coleman and M. S. Strano, *Nat. Nanotechnol.*, 2012, **7**, 699–712.
7 Z. Y. Yin, X. Zhang, Y. Q. Cai, J. Z. Chen, J. I. Wong, Y. Y. Tay, J. W. Chai, J. M. T. Wu, Z. Y. Zeng, B. Zheng, H. Y. Yang and H. Zhang, *Angew. Chem., Int. Ed.*, 2014, **53**, 12560–12565.
8 Z. Y. Yin, H. Li, L. Jiang, Y. M. Shi, Y. H. Sun, G. Lu, Q. Zhang, X. D. Chen and H. Zhang, *ACS Nano*, 2012, **6**, 74–80.
9 F. Bonaccorso, Z. Sun, T. Hasan and A. C. Ferrari, *Nat. Photonics*, 2010, **4**, 611–622.
10 J.-F. Ge, Z.-L. Liu, C. Liu, C.-L. Gao, D. Qian, Q.-K. Xue, Y. Liu and J.-F. Jia, *Nat. Mater.*, 2015, **14**, 285–289.
11 A. N. Grigorenko, M. Polini and K. S. Novoselov, *Nat. Photonics*, 2012, **6**, 749–758.
12 D. Deng, K. S. Novoselov, Q. Fu, N. Zheng, Z. Tian and X. Bao, *Nat. Nanotechnol.*, 2016, **11**, 218–230.
13 Z. Y. Yin, B. Chen, M. Bosman, X. H. Cao, J. Z. Chen, B. Zheng and H. Zhang, *Small*, 2014, **10**, 3537–3543.
14 W. J. Zhou, Z. Y. Yin, Y. P. Du, X. Huang, Z. Y. Zeng, Z. X. Fan, H. Liu, J. Y. Wang and H. Zhang, *Small*, 2013, **9**, 140–147.
15 C. L. Tan and H. Zhang, *Chem. Soc. Rev.*, 2015, **44**, 2713–2731.
16 J. Z. Chen, X. J. Wu, L. S. Yin, B. Li, X. Hong, Z. X. Fan, B. Chen, C. Xue and H. Zhang, *Angew. Chem., Int. Ed.*, 2015, **54**, 1210–1214.
17 Z. Y. Zeng, C. L. Tan, X. Huang, S. Y. Bao and H. Zhang, *Energy Environ. Sci.*, 2014, **7**, 797–803.
18 X. Huang, Z. Y. Zeng, S. Y. Bao, M. F. Wang, X. Y. Qi, Z. X. Fan and H. Zhang, *Nat. Commun.*, 2013, **4**, 1444.
19 W. Wu, L. Wang, Y. Li, F. Zhang, L. Lin, S. Niu, D. Chenet, X. Zhang, Y. Hao, T. F. Heinz, J. Hone and Z. L. Wang, *Nature*, 2014, **514**, 470–474.
20 D. Chen, L. Tang and J. Li, *Chem. Soc. Rev.*, 2010, **39**, 3157–3180.
21 R. Raccichini, A. Varzi, S. Passerini and B. Scrosati, *Nat. Mater.*, 2015, **14**, 271–279.
22 C. H. Xu, B. H. Xu, Y. Gu, Z. G. Xiong, J. Sun and X. S. Zhao, *Energy Environ. Sci.*, 2013, **6**, 1388–1414.
23 X. Huang, C. L. Tan, Z. Y. Yin and H. Zhang, *Adv. Mater.*, 2014, **26**, 2185–2204.
24 X. Cao, C. Tan, X. Zhang, W. Zhao and H. Zhang, *Adv. Mater.*, 2016, **28**, 6167–6196.
25 S. Bae, H. Kim, Y. Lee, X. Xu, J.-S. Park, Y. Zheng, J. Balakrishnan, T. Lei, H. Ri Kim, Y. I. Song, Y.-J. Kim, K. S. Kim, B. Ozyilmaz, J.-H. Ahn, B. H. Hong and S. Iijima, *Nat. Nanotechnol.*, 2010, **5**, 574–578.
26 X. L. Li, X. R. Wang, L. Zhang, S. W. Lee and H. J. Dai, *Science*, 2008, **319**, 1229–1232.
27 X. Zhang, Z. C. Lai, Z. D. Liu, C. L. Tan, Y. Huang, B. Li, M. T. Zhao, L. H. Xie, W. Huang and H. Zhang, *Angew. Chem., Int. Ed.*, 2015, **54**, 5425–5428.
28 X. Zhang, H. M. Xie, Z. D. Liu, C. L. Tan, Z. M. Luo, H. Li, J. D. Lin, L. Q. Sun, W. Chen, Z. C. Xu, L. H. Xie, W. Huang and H. Zhang, *Angew. Chem., Int. Ed.*, 2015, **54**, 3653–3657.
29 A. K. Geim and I. V. Grigorieva, *Nature*, 2013, **499**, 419–425.
30 Y. Gong, J. Lin, X. Wang, G. Shi, S. Lei, Z. Lin, X. Zou, G. Ye, R. Vajtai, B. I. Yakobson, H. Terrones, M. Terrones, B. K. Tay, J. Lou, S. T. Pantelides, Z. Liu, W. Zhou and P. M. Ajayan, *Nat. Mater.*, 2014, **13**, 1135–1142.
31 J. Zhao, Q. M. Deng, A. Bachmatiuk, G. Sandeep, A. Popov, J. Eckert and M. H. Rummeli, *Science*, 2014, **343**, 1228–1232.
32 J. Kang, S. Tongay, J. Li and J. Wu, *J. Appl. Phys.*, 2013, **113**, 143703.
33 Y. Yu, F. Yang, X. F. Lu, Y. J. Yan, Y.-H. Cho, L. Ma, X. Niu, S. Kim, Y.-W. Son, D. Feng, S. Li, S.-W. Cheong, X. H. Chen and Y. Zhang, *Nat. Nanotechnol.*, 2015, **10**, 270–276.
34 Z. Zeng, Z. Yin, X. Huang, H. Li, Q. He, G. Lu, F. Boey and H. Zhang, *Angew. Chem., Int. Ed.*, 2011, **50**, 11093–11097.
35 Z. Zeng, T. Sun, J. Zhu, X. Huang, Z. Yin, G. Lu, Z. Fan, Q. Yan, H. H. Hng and H. Zhang, *Angew. Chem., Int. Ed.*, 2012, **51**, 9052–9056.
36 C. L. Tan, W. Zhao, A. Chaturvedi, Z. Fei, Z. Y. Zeng, J. Z. Chen, Y. Huang, P. Ercius, Z. M. Luo, X. Y. Qi, B. Chen, Z. C. Lai, B. Li, X. Zhang, J. Yang, Y. Zong, C. H. Jin, H. M. Zheng, C. Kloc and H. Zhang, *Small*, 2016, **12**, 1866–1874.
37 W. Bao, J. Wan, X. Han, X. Cai, H. Zhu, D. Kim, D. Ma, Y. Xu, J. N. Munday, H. D. Drew, M. S. Fuhrer and L. Hu, *Nat. Commun.*, 2014, **5**, 4224.
38 F. Wang, Y. Zhang, C. Tian, C. Girit, A. Zettl, M. Crommie and Y. R. Shen, *Science*, 2008, **320**, 206–209.
39 Z. Q. Li, E. A. Henriksen, Z. Jiang, Z. Hao, M. C. Martin, P. Kim, H. L. Stormer and D. N. Basov, *Nat. Phys.*, 2008, **4**, 532–535.
40 W. Bao, L. Jing, J. Velasco, Jr., Y. Lee, G. Liu, D. Tran, B. Standley, M. Aykol, S. B. Cronin, D. Smirnov, M. Koshino, E. McCann, M. Bockrath and C. N. Lau, *Nat. Phys.*, 2011, **7**, 948–952.
41 J. Feng, X. Qian, C.-W. Huang and J. Li, *Nat. Photonics*, 2012, **6**, 865–871.
42 K. F. Mak, C. Lee, J. Hone, J. Shan and T. F. Heinz, *Phys. Rev. Lett.*, 2010, **105**, 136805.
43 M. S. Dresselhaus and G. Dresselhaus, *Adv. Phys.*, 2002, **51**, 1–186.
44 E. Benavente, M. A. Santa Ana, F. Mendizabal and G. Gonzalez, *Coord. Chem. Rev.*, 2002, **224**, 87–109.

 This journal is © The Royal Society of Chemistry 2016

Published on 05 October 2016. Downloaded by Xiamen University on 23/11/2017 07:01:38.

45 *Intercalated Layered Materials*, ed. F. Lévy, D. Reidel Publishing Company, Dordrecht, Holland, 1979.
46 M. Winter, J. O. Besenhard, M. E. Spahr and P. Novak, *Adv. Mater.*, 1998, **10**, 725–763.
47 M. S. Whittingham, *Prog. Solid State Chem.*, 1978, **12**, 41–99.
48 R. H. Friend and A. D. Yoffe, *Adv. Phys.*, 1987, **36**, 1–94.
49 I. Prigogine and S. A. Rice, *Adv. Chem. Phys.*, 1982, **49**, 455–532.
50 H. Wang, Z. Lu, S. Xu, D. Kong, J. J. Cha, G. Zheng, P.-C. Hsu, K. Yan, D. Bradshaw, F. B. Prinz and Y. Cui, *Proc. Natl. Acad. Sci. U. S. A.*, 2013, **110**, 19701–19706.
51 R. Kappera, D. Voiry, S. E. Yalcin, B. Branch, G. Gupta, A. D. Mohite and M. Chhowalla, *Nat. Mater.*, 2014, **13**, 1128–1134.
52 T. H. Bointon, I. Khrapach, R. Yakimova, A. V. Shytov, M. F. Craciun and S. Russo, *Nano Lett.*, 2014, **14**, 1751–1755.
53 E. Morosan, H. W. Zandbergen, L. Li, M. Lee, J. G. Checkelsky, M. Heinrich, T. Siegrist, N. P. Ong and R. J. Cava, *Phys. Rev. B: Condens. Matter Mater. Phys.*, 2007, **75**, 104401.
54 C. Wan, X. Gu, F. Dang, T. Itoh, Y. Wang, H. Sasaki, M. Kondo, K. Koga, K. Yabuki, G. J. Snyder, R. Yang and K. Koumoto, *Nat. Mater.*, 2015, **14**, 622–627.
55 J. Wan, W. Bao, Y. Liu, J. Dai, F. Shen, L. Zhou, X. Cai, D. Urban, Y. Li, K. Jungjohann, M. S. Fuhrer and L. Hu, *Adv. Energy Mater.*, 2015, **5**, 1401742.
56 D. C. Lin, Y. Y. Liu, Z. Liang, H. W. Lee, J. Sun, H. T. Wang, K. Yan, J. Xie and Y. Cui, *Nat. Nanotechnol.*, 2016, **11**, 626–632.
57 D. Voiry, R. Fullon, J. Yang, C. de Carvalho Castro e Silva, R. Kappera, I. Bozkurt, D. Kaplan, M. J. Lagos, P. E. Batson, G. Gupta, A. D. Mohite, L. Dong, D. Er, V. B. Shenoy, T. Asefa and M. Chhowalla, *Nat. Mater.*, 2016, **15**, 1003–1009.
58 K. S. Novoselov, D. Jiang, F. Schedin, T. J. Booth, V. V. Khotkevich, S. V. Morozov and A. K. Geim, *Proc. Natl. Acad. Sci. U. S. A.*, 2005, **102**, 10451–10453.
59 K. S. Novoselov, A. K. Geim, S. V. Morozov, D. Jiang, Y. Zhang, S. V. Dubonos, I. V. Grigorieva and A. A. Firsov, *Science*, 2004, **306**, 666–669.
60 S. D. Lacey, J. Y. Wan, A. V. Cresce, S. M. Russell, J. Q. Dai, W. Z. Bao, K. Xu and L. B. Hu, *Nano Lett.*, 2015, **15**, 1018–1024.
61 M. Z. Cai, D. Thorpe, D. H. Adamson and H. C. Schniepp, *J. Mater. Chem.*, 2012, **22**, 24992–25002.
62 X. S. Li, W. W. Cai, J. H. An, S. Kim, J. Nah, D. X. Yang, R. Piner, A. Velamakanni, I. Jung, E. Tutuc, S. K. Banerjee, L. Colombo and R. S. Ruoff, *Science*, 2009, **324**, 1312–1314.
63 S. Bae, H. Kim, Y. Lee, X. F. Xu, J. S. Park, Y. Zheng, J. Balakrishnan, T. Lei, H. R. Kim, Y. I. Song, Y. J. Kim, K. S. Kim, B. Ozyilmaz, J. H. Ahn, B. H. Hong and S. Iijima, *Nat. Nanotechnol.*, 2010, **5**, 574–578.
64 M. Chhowalla, H. S. Shin, G. Eda, L. J. Li, K. P. Loh and H. Zhang, *Nat. Chem.*, 2013, **5**, 263–275.
65 X. S. Li, C. W. Magnuson, A. Venugopal, R. M. Tromp, J. B. Hannon, E. M. Vogel, L. Colombo and R. S. Ruoff, *J. Am. Chem. Soc.*, 2011, **133**, 2816–2819.
66 Y. Gao, W. C. Ren, T. Ma, Z. B. Liu, Y. Zhang, W. B. Liu, L. P. Ma, X. L. Ma and H. M. Cheng, *ACS Nano*, 2013, **7**, 5199–5206.
67 J. H. Park, J. C. Park, S. J. Yun, H. Kim, D. H. Luong, S. M. Kim, S. H. Choi, W. Yang, J. Kong, K. K. Kim and Y. H. Lee, *ACS Nano*, 2014, **8**, 8520–8528.
68 Y. H. Lee, X. Q. Zhang, W. J. Zhang, M. T. Chang, C. T. Lin, K. D. Chang, Y. C. Yu, J. T. W. Wang, C. S. Chang, L. J. Li and T. W. Lin, *Adv. Mater.*, 2012, **24**, 2320–2325.
69 A. M. van der Zande, P. Y. Huang, D. A. Chenet, T. C. Berkelbach, Y. M. You, G. H. Lee, T. F. Heinz, D. R. Reichman, D. A. Muller and J. C. Hone, *Nat. Mater.*, 2013, **12**, 554–561.
70 Y. J. Zhan, Z. Liu, S. Najmaei, P. M. Ajayan and J. Lou, *Small*, 2012, **8**, 966–971.
71 X. S. Li, C. W. Magnuson, A. Venugopal, J. H. An, J. W. Suk, B. Y. Han, M. Borysiak, W. W. Cai, A. Velamakanni, Y. W. Zhu, L. F. Fu, E. M. Vogel, E. Voelkl, L. Colombo and R. S. Ruoff, *Nano Lett.*, 2010, **10**, 4328–4334.
72 J. W. Suk, A. Kitt, C. W. Magnuson, Y. F. Hao, S. Ahmed, J. H. An, A. K. Swan, B. B. Goldberg and R. S. Ruoff, *ACS Nano*, 2011, **5**, 6916–6924.
73 G. Deokar, J. Avila, I. Razado-Colambo, J. L. Codron, C. Boyaval, E. Galopin, M. C. Asensio and D. Vignaud, *Carbon*, 2015, **89**, 82–92.
74 A. Reina, X. T. Jia, J. Ho, D. Nezich, H. B. Son, V. Bulovic, M. S. Dresselhaus and J. Kong, *Nano Lett.*, 2009, **9**, 30–35.
75 J. N. Coleman, M. Lotya, A. O'Neill, S. D. Bergin, P. J. King, U. Khan, K. Young, A. Gaucher, S. De, R. J. Smith, I. V. Shvets, S. K. Arora, G. Stanton, H. Y. Kim, K. Lee, G. T. Kim, G. S. Duesberg, T. Hallam, J. J. Boland, J. J. Wang, J. F. Donegan, J. C. Grunlan, G. Moriarty, A. Shmeliov, R. J. Nicholls, J. M. Perkins, E. M. Grieveson, K. Theuwissen, D. W. McComb, P. D. Nellist and V. Nicolosi, *Science*, 2011, **331**, 568–571.
76 Y. Hernandez, V. Nicolosi, M. Lotya, F. M. Blighe, Z. Y. Sun, S. De, I. T. McGovern, B. Holland, M. Byrne, Y. K. Gun'ko, J. J. Boland, P. Niraj, G. Duesberg, S. Krishnamurthy, R. Goodhue, J. Hutchison, V. Scardaci, A. C. Ferrari and J. N. Coleman, *Nat. Nanotechnol.*, 2008, **3**, 563–568.
77 U. Khan, A. O'Neill, M. Lotya, S. De and J. N. Coleman, *Small*, 2010, **6**, 864–871.
78 A. O'Neill, U. Khan, P. N. Nirmalraj, J. Boland and J. N. Coleman, *J. Phys. Chem. C*, 2011, **115**, 5422–5428.
79 K. R. Paton, E. Varrla, C. Backes, R. J. Smith, U. Khan, A. O'Neill, C. Boland, M. Lotya, O. M. Istrate, P. King, T. Higgins, S. Barwich, P. May, P. Puczkarski, I. Ahmed, M. Moebius, H. Pettersson, E. Long, J. Coelho, S. E. O'Brien, E. K. McGuire, B. M. Sanchez, G. S. Duesberg, N. McEvoy, T. J. Pennycook, C. Downing, A. Crossley, V. Nicolosi and J. N. Coleman, *Nat. Mater.*, 2014, **13**, 624–630.
80 X. X. Liu, J. L. Liu, D. Zhan, J. X. Yan, J. Wang, D. L. Chao, L. F. Lai, M. H. Chen, J. H. Yin and Z. X. Shen, *RSC Adv.*, 2013, **3**, 11601–11606.
81 K. G. Zhou, N. N. Mao, H. X. Wang, Y. Peng and H. L. Zhang, *Angew. Chem., Int. Ed.*, 2011, **50**, 10839–10842.
82 J. N. Coleman, *Acc. Chem. Res.*, 2013, **46**, 14–22.

Published on 05 October 2016. Downloaded by Xiamen University on 23/11/2017 07:01:38.

83 D. A. Dikin, S. Stankovich, E. J. Zimney, R. D. Piner, G. H. B. Dommett, G. Evmenenko, S. T. Nguyen and R. S. Ruoff, *Nature*, 2007, **448**, 457–460.
84 V. Nicolosi, M. Chhowalla, M. G. Kanatzidis, M. S. Strano and J. N. Coleman, *Science*, 2013, **340**, 1420.
85 C. Y. Zhi, Y. Bando, C. C. Tang, H. Kuwahara and D. Golberg, *Adv. Mater.*, 2009, **21**, 2889–2893.
86 D. C. Marcano, D. V. Kosynkin, J. M. Berlin, A. Sinitskii, Z. Sun, A. Slesarev, L. B. Alemany, W. Lu and J. M. Tour, *ACS Nano*, 2010, **4**, 4806–4814.
87 M. Naguib and Y. Gogotsi, *Acc. Chem. Res.*, 2015, **48**, 128–135.
88 A. O'Neill, U. Khan and J. N. Coleman, *Chem. Mater.*, 2012, **24**, 2414–2421.
89 L. T. Dou, A. B. Wong, Y. Yu, M. L. Lai, N. Kornienko, S. W. Eaton, A. Fu, C. G. Bischak, J. Ma, T. N. Ding, N. S. Ginsberg, L. W. Wang, A. P. Alivisatos and P. D. Yang, *Science*, 2015, **349**, 1518–1521.
90 C. Faugeras, A. Nerriere, M. Potemski, A. Mahmood, E. Dujardin, C. Berger and W. A. de Heer, *Appl. Phys. Lett.*, 2008, **92**, 011914.
91 C. L. Tan and H. Zhang, *Nat. Commun.*, 2015, **6**, 7873.
92 D. Voiry, M. Salehi, R. Silva, T. Fujita, M. Chen, T. Asefa, V. B. Shenoy, G. Eda and M. Chhowalla, *Nano Lett.*, 2013, **13**, 6222–6227.
93 I. Khrapach, F. Withers, T. H. Bointon, D. K. Polyushkin, W. L. Barnes, S. Russo and M. F. Craciun, *Adv. Mater.*, 2012, **24**, 2844–2849.
94 D. Voiry, H. Yamaguchi, J. Li, R. Silva, D. C. B. Alves, T. Fujita, M. Chen, T. Asefa, V. B. Shenoy, G. Eda and M. Chhowalla, *Nat. Mater.*, 2013, **12**, 850–855.
95 K. J. Koski, C. D. Wessells, B. W. Reed, J. J. Cha, D. S. Kong and Y. Cui, *J. Am. Chem. Soc.*, 2012, **134**, 13773–13779.
96 H. T. Yuan, H. T. Wang and Y. Cui, *Acc. Chem. Res.*, 2015, **48**, 81–90.
97 J. P. Motter, K. J. Koski and Y. Cui, *Chem. Mater.*, 2014, **26**, 2313–2317.
98 N. I. Kovtyukhova, Y. X. Wang, R. T. Lv, M. Terrones, V. H. Crespi and T. E. Mallouk, *J. Am. Chem. Soc.*, 2013, **135**, 8372–8381.
99 T. Ohzuku, Y. Iwakoshi and K. Sawai, *J. Electrochem. Soc.*, 1993, **140**, 2490–2498.
100 J. A. Seel and J. R. Dahn, *J. Electrochem. Soc.*, 2000, **147**, 892–898.
101 W. Z. Bao, G. Liu, Z. Zhao, H. Zhang, D. Yan, A. Deshpande, B. J. LeRoy and C. N. Lau, *Nano Res.*, 2010, **3**, 98–102.
102 S. D. Lacey, J. Wan, A. v. W. Cresce, S. M. Russell, J. Dai, W. Bao, K. Xu and L. Hu, *Nano Lett.*, 2015, **15**, 1018–1024.
103 M. Inaba, H. Yoshida, Z. Ogumi, T. Abe, Y. Mizutani and M. Asano, *J. Electrochem. Soc.*, 1995, **142**, 20–26.
104 W. J. Zhao, P. H. Tan, J. Liu and A. C. Ferrari, *J. Am. Chem. Soc.*, 2011, **133**, 5941–5946.
105 D. Zhan, L. Sun, Z. H. Ni, L. Liu, X. F. Fan, Y. Wang, T. Yu, Y. M. Lam, W. Huang and Z. X. Shen, *Adv. Funct. Mater.*, 2010, **20**, 3504–3509.
106 F. P. Campana, R. Kotz, J. Vetter, P. Novak and H. Siegenthaler, *Electrochem. Commun.*, 2005, **7**, 107–112.
107 D. Alliata, R. Kotz, O. Haas and H. Siegenthaler, *Langmuir*, 1999, **15**, 8483–8489.
108 F. P. Campana, H. Buqa, P. Novak, R. Kotz and H. Siegenthaler, *Electrochem. Commun.*, 2008, **10**, 1590–1593.
109 J. Park, J. S. Kim, J. W. Park, T. H. Nam, K. W. Kim, J. H. Ahn, G. Wang and H. J. Ahn, *Electrochim. Acta*, 2013, **92**, 427–432.
110 X. H. Liu, J. W. Wang, Y. Liu, H. Zheng, A. Kushima, S. Huang, T. Zhu, S. X. Mao, J. Li, S. L. Zhang, W. Lu, J. M. Tour and J. Y. Huang, *Carbon*, 2012, **50**, 3836–3844.
111 K. Kanetani, K. Sugawara, T. Sato, R. Shimizu, K. Iwaya, T. Hitosugi and T. Takahashi, *Proc. Natl. Acad. Sci. U. S. A.*, 2012, **109**, 19610–19613.
112 E. W. Ong, M. J. McKelvy, G. Ouvrard and W. S. Glaunsinger, *Chem. Mater.*, 1992, **4**, 14–17.
113 P. Ganal, P. Moreau, G. Ouvrard, M. Sidorov, M. McKelvy and W. Glaunsinger, *Chem. Mater.*, 1995, **7**, 1132–1139.
114 J. Ye, M. F. Craciun, M. Koshino, S. Russo, S. Inoue, H. Yuan, H. Shimotani, A. F. Morpurgo and Y. Iwasa, *Proc. Natl. Acad. Sci. U. S. A.*, 2011, **108**, 13002–13006.
115 J. T. Ye, Y. J. Zhang, R. Akashi, M. S. Bahramy, R. Arita and Y. Iwasa, *Science*, 2012, **338**, 1193–1196.
116 W. Bao, Z. Fang, J. Wan, J. Dai, H. Zhu, X. Han, X. Yang, C. Preston and L. Hu, *ACS Nano*, 2014, 10606–10612.
117 N. Kim, K. S. Kim, N. Jung, L. Brus and P. Kim, *Nano Lett.*, 2011, **11**, 860–865.
118 G. Csanyi, P. B. Littlewood, A. H. Nevidomskyy, C. J. Pickard and B. D. Simons, *Nat. Phys.*, 2005, **1**, 42–45.
119 T. E. Weller, M. Ellerby, S. S. Saxena, R. P. Smith and N. T. Skipper, *Nat. Phys.*, 2005, **1**, 39–41.
120 G. Profeta, M. Calandra and F. Mauri, *Nat. Phys.*, 2012, **8**, 131–134.
121 E. R. Margine, H. Lambert and F. Giustino, *Sci. Rep.*, 2016, **6**, 21414.
122 J.-H. Chen, C. Jang, S. Xiao, M. Ishigami and M. S. Fuhrer, *Nat. Nanotechnol.*, 2008, **3**, 206–209.
123 A. H. Castro Neto, F. Guinea, N. M. R. Peres, K. S. Novoselov and A. K. Geim, *Rev. Mod. Phys.*, 2009, **81**, 109–162.
124 F. Xiong, H. Wang, X. Liu, J. Sun, M. Brongersma, E. Pop and Y. Cui, *Nano Lett.*, 2015, **15**, 6777–6784.
125 R. Y. Zhang, I. L. Tsai, J. Chapman, E. Khestanova, J. Waters and I. V. Grigorieva, *Nano Lett.*, 2016, **16**, 629–636.
126 Q. Bao and K. P. Loh, *ACS Nano*, 2012, **6**, 3677–3694.
127 H. A. Becerril, J. Mao, Z. Liu, R. M. Stoltenberg, Z. Bao and Y. Chen, *ACS Nano*, 2008, **2**, 463–470.
128 J. Y. Wan, F. Gu, W. Z. Bao, J. Q. Dai, F. Shen, W. Luo, X. G. Han, D. Urban and L. B. Hu, *Nano Lett.*, 2015, **15**, 3763–3769.
129 D. J. Wehenkel, T. H. Bointon, T. Booth, P. Boggild, M. F. Craciun and S. Russo, *Sci. Rep.*, 2015, **5**, 7609.
130 T. H. Bointon, G. F. Jones, A. De Sanctis, R. Hill-Pearce, M. F. Craciun and S. Russo, *Sci. Rep.*, 2015, **5**, 16464.
131 F. Withers, T. H. Bointon, M. F. Craciun and S. Russo, *ACS Nano*, 2013, **7**, 5052–5057.
132 Y. S. Guo, D. Z. Sun, B. Ouyang, A. Raja, J. Song, T. F. Heinz and L. E. Brus, *Nano Lett.*, 2015, **15**, 5081–5088.

 This journal is © The Royal Society of Chemistry 2016

Published on 05 October 2016. Downloaded by Xiamen University on 23/11/2017 07:01:38.

133 G. Eda, H. Yamaguchi, D. Voiry, T. Fujita, M. W. Chen and M. Chhowalla, *Nano Lett.*, 2011, **11**, 5111–5116.
134 Y. Wang, J. Z. Ou, S. Balendhran, A. F. Chrimes, M. Mortazavi, D. D. Yao, M. R. Field, K. Latham, V. Bansal, J. R. Friend, S. Zhuiykov, N. V. Medhekar, M. S. Strano and K. Kalantar-zadeh, *ACS Nano*, 2013, **7**, 10083–10093.
135 J. Z. Ou, A. F. Chrimes, Y. C. Wang, S. Y. Tang, M. S. Strano and K. Kalantar-zadeh, *Nano Lett.*, 2014, **14**, 857–863.
136 J. Yao, K. J. Koski, W. Luo, J. J. Cha, L. Hu, D. Kong, V. K. Narasimhan, K. Huo and Y. Cui, *Nat. Commun.*, 2014, **5**, 5670.
137 J. J. Cha, K. J. Koski, K. C. Y. Huang, K. X. Wan, W. Luo, D. Kong, Z. Yu, S. Fan, M. L. Brongersma and Y. Cui, *Nano Lett.*, 2013, **13**, 5913–5918.
138 K. J. Koski, C. D. Wessells, B. W. Reed, J. J. Cha, D. Kong and Y. Cui, *J. Am. Chem. Soc.*, 2012, **134**, 13773–13779.
139 K. P. Chen, F. R. Chung, M. Wang and K. J. Koski, *J. Am. Chem. Soc.*, 2015, **137**, 5431–5437.
140 M. Wang and K. J. Koski, *ACS Nano*, 2015, **9**, 3226–3233.
141 A. A. Balandin, *Nat. Mater.*, 2011, **10**, 569–581.
142 A. A. Balandin, *MRS Bull.*, 2014, **39**, 817–823.
143 C. Wan, Y. Wang, N. Wang, W. Norimatsu, M. Kusunoki and K. Koumoto, *J. Electron. Mater.*, 2011, **40**, 1271–1280.
144 J. Cho, M. D. Losego, H. G. Zhang, H. Kim, J. Zuo, I. Petrov, D. G. Cahill and P. V. Braun, *Nat. Commun.*, 2014, **5**, 4035.
145 W. J. Hardy, C.-W. Chen, A. Marcinkova, H. Ji, J. Sinova, D. Natelson and E. Morosan, *Phys. Rev. B: Condens. Matter Mater. Phys.*, 2015, **91**, 054426.
146 C. K. Chan, H. Peng, G. Liu, K. McIlwrath, X. F. Zhang, R. A. Huggins and Y. Cui, *Nat. Nanotechnol.*, 2008, **3**, 31–35.
147 P. Simon and Y. Gogotsi, *Nat. Mater.*, 2008, **7**, 845–854.
148 J. Wan, A. F. Kaplan, J. Zheng, X. Han, Y. Chen, N. J. Weadock, N. Faenza, S. Lacey, T. Li, J. Guo and L. Hu, *J. Mater. Chem. A*, 2014, **2**, 6051–6057.
149 M. Acerce, D. Voiry and M. Chhowalla, *Nat. Nanotechnol.*, 2015, **10**, 313–318.
150 M. A. Lukowski, A. S. Daniel, C. R. English, F. Meng, A. Forticaux, R. J. Hamers and S. Jin, *Energy Environ. Sci.*, 2014, **7**, 2608–2613.
151 J. Kibsgaard, Z. Chen, B. N. Reinecke and T. F. Jaramillo, *Nat. Mater.*, 2012, **11**, 963–969.
152 M. A. Lukowski, A. S. Daniel, F. Meng, A. Forticaux, L. Li and S. Jin, *J. Am. Chem. Soc.*, 2013, **135**, 10274–10277.
153 H. Wang, Z. Lu, D. Kong, J. Sun, T. M. Hymel and Y. Cui, *ACS Nano*, 2014, **8**, 4940–4947.
154 Z. Lu, H. Wang, D. Kong, K. Yan, P.-C. Hsu, G. Zheng, H. Yao, Z. Liang, X. Sun and Y. Cui, *Nat. Commun.*, 2014, **5**, 4345.
155 J. W. Yang, G. Lee, J. S. Kim and K. S. Kim, *J. Phys. Chem. Lett.*, 2011, **2**, 2577–2581.
156 D. Zhan, J. X. Yan, Z. H. Ni, L. Sun, L. F. Lai, L. Liu, X. Y. Liu and Z. X. Shen, *Small*, 2015, **11**, 1177–1182.
157 S. N. Shirodkar and E. Kaxiras, *Phys. Rev. B: Condens. Matter Mater. Phys.*, 2016, **93**, 245438.
158 Y. Liu, Z. Xu, J. Zhan, P. Li and C. Gao, *Adv. Mater.*, 2016, **28**, 7941–7947.